ENHANCING CHIROPTICAL SIGNALS FROM METAMATERIALS VIA NONLINEAR EXCITATION

A Thesis
Presented to
The Academic Faculty

By

Sean P. Rodrigues

In Partial Fulfillment
of the Requirements for the
Master's Degree in the
School of Materials Science & Engineering

Georgia Institute of Technology
December 2015

Copyright © by Sean Rodrigues 2015

ENHANCING CHIROPTICAL SIGNALS FROM METAMATERIALS VIA NONLINEAR EXCITATION

Approved by:

Dr. Wenshan Cai, Advisor
School of Electrical & Computer Engineering
Jointly School of Materials Science and Engineering
Georgia Institute of Technology

Dr. Vladimir Tsukruk
School of Materials Science & Engineering
Georgia Institute of Technology

Dr. Mohan Srinivasarao
School of Materials Science & Engineering
Georgia Institute of Technology

Date Approved: 11/10/2015

To my grandparents and family,

Whose endless love and support made this work possible.

ACKNOWLEDGEMENTS

I would like to thank my advisor Wenshan Cai. His advocacy and his relentless desire to help me achieve my goals is more than I imagined in an advisor and I'm undeniably thankful. I'm indebted to the dedication of my labmates, Shoufeng Lan, Yonghao Cui and Lei Kang. I cannot speak enough to their guidance, support and vast knowledge of the field. Thank you so much for being the best team I have ever worked with.. I would also like to thank my thesis committee Dr. Mohan Srinivasarao & Dr. Vladimir Tsukruk for their support towards this work and beyond.

I wouldn't be in graduate school if it wasn't for the amazing mentorship I've had from mentors at my alma mater: Dr. Lukas Novotny, Dr. Matthew Yates, Dr. James Farrar and Nicholas Valentino.

Thank you to the National Science Foundation (NSF) Graduate Research Fellowship for funding me under Grant No. DGE-1148903. Thank you to the Goizueta Foundation for supporting me via the GoSTEM Fellowship.

With the outmost gratitude and love, I thank my mother for insisting that I pursue my dreams no matter the cost. I want to thank the rest of my family, Rianna, Justin and Joe : I may not have been physically present while I've been obtaining my degrees, but I'm indebted for your kindness and understanding.

TABLE OF CONTENTS

LIST OF FIGURES

Page

LIST OF SYMBOLS AND ABBREVIATIONS

CD	Circular Dichroism
OR	Optical Rotation
SHG	Second Harmonic Generation
SHG-CD	Second Harmonic Generation – Circular Dichroism
TPL	Two Photon Luminescence
TPL-CD	Two Photon Luminescence – Circular Dichroism
NIR	Near-Infrared

SUMMARY

As natural chiral materials demonstrate limited circularly dichroic contrasts, enhancement of these polarization dependent signals has been the focus of chiral metamaterial research. By manipulating the geometric chirality of resonant plasmonic nanostructures, we are capable of enhancing light confinement to amplify chiral modified, nonlinear signals from quantum emitters. The metamaterial demonstrates a linear transmission contrast of 0.5 between left and right circular polarizations and a 20× contrast between second harmonic responses from the two incident polarizations. Nonlinear and linear response images probed with circularly polarized lights show strongly defined contrast. As a second set of experimentation, the chiral center of the metamaterial is opened, providing direct access to place emitters to occupy the most light-confining and chirally sensitive regions. The resulting two-photon emission profiles from circularly polarized excitation displays mirrored symmetry for the two enantiomer structures. The efficiency of the nonlinear signal directly correlates to the chiral resonance of the linear regime. The nonlinear emission signal is enhanced by 40× that of the emitters not embedded in the metamaterial and displays a 3× contrast for the opposite circular polarization. Such manipulations of nonlinear signals with metamaterials open pathways for diverse applications where chiral selective signals are monitored, processed, and analyzed.

Foreword

The materials implemented in optics to control the flow of light have undergone many progressions, but the fundamental roles they play have remained the same until more recently. When we turn on a light or other source, it illuminates a space or material through which we can detect that light. In this most basic sense, light is a tool through which we gain information via illumination and detection. Over the years, our devices used for the generation and capture of light have become ever more advanced, as shown by our ability to produce, switch and detect signals on time scales smaller than we could have imagined and at orders of magnitudes larger and smaller than possible with our eyes. Most important in our use of light today, is how we manipulate it. As our source and detection systems become of exceedingly higher quality, we must ask ourselves "What effects can we achieve in the modification of light prior to its consumed end state?" The state of light between the moment it is sensed and the time it is generated is becoming ever more crucial. Upper bounds on the physical limitations of our sources and detectors are becoming more prominent, causing us to rely more heavily on tools to manifest how light operates as it is transferred

from point A to B. These tools including nonlinear optics, liquid crystals, electrooptic modulators, etc. have revolutionized the utility of light and are becoming ubiquitous in common place society.

In the realm of electromagnetics, we have recognized that in order to manipulate light, we must utilize structures that can interact with the wave vector of light on its fundamental length scale. This understanding led us to investigate and engineer photonic crystals – a method to manipulate light with structures that have dimensions on the same order of magnitude of the wavelength of light or slightly larger. In the 1950's, the realm of plasmonics was being recognized by Ritchie and Turbadar for its ability to confine light on smaller length scales. In order, to bend light even further into directions not predicted by classical optics, light had to be manipulated with unit cells not so small that they were individually undetectable to a single wavelength, like an atom, but not so large that they would be limited by classical geometric optics. The space in-between is left to a field called metamaterials, a class of material that hybridizes different classes of materials in an architectural manner to manipulate the propagation of light in methods beyond what was perceived in the realm of classical optics. Optical metamaterials, also known as plasmonic metamaterials is a class of materials that exploits the plasmonic features of

metals interwoven into dielectric components to confine and bend light to provide unforeseen properties in the far field. The recent birth of optical metamaterials has paved the way for technologies such as negative refraction, ultrafast optical data processing and even the possibility of invisibility. The exotic features of these materials have enticed researchers to steer their focus into the domain of metamaterials. An all-encompassing resource on metamaterials was published in 2010 and is capable of bringing scientists up to par with the field.[1]

A few years back a perspective piece on the future of metamaterials was released.[2] The article provided a broad genre of research topics that had been and were needed to be studied within the field of metamaterials. While the guide remains an outstanding resource to return to when trying to piece the future of the field together, the outline remains a poster board for some of the hot topics in the field. The true potential of metamaterials can only be extracted upon the integration of many of these thrusts.

Just as metamaterials intertwine two types of fundamentally different materials, the future of research relies on the entanglement of unexpected fields. In this thesis, theoretical and experimental results are presented on the intersection of chiral and nonlinear metamaterials. Chirality is a property that can be structurally engineered to affect how a material will interact with incident

electromagnetic fields. In the context of this research, the subject of nonlinearity utilizes a fundamental high intensity beam and a material's nonlinear refractive index or portion of its susceptibility tensor. The intersection of these two fields seeks to enhance the chiral features presented by these materials and to enhance, extract, and access new properties of the material. The second chapter of this thesis utilizes the chiral nature of a twisted arc metamaterial structure in conjunction with a high powered nonlinear laser to produce a second harmonic signal. The emitted second harmonic signal demonstrates dependence on the type of circular irradiation, with spectroscopic characteristics nearly identical to that of its linear counterpart. The nonlinear response shows magnified contrast between the two opposing circular polarizations. A great deal of the information presented in chapter two can be found in the journal article "Nonlinear imaging and spectroscopy of chiral metamaterials" as published in *Advanced Materials*.[3] The third chapter utilities circularly dependent hotspots within a similar metamaterial structure to demonstrate enhanced luminescent properties. The extraction of this chiral property with such an intense enhancement will be crucial to the development of hybrid active-metamaterial structures. A large portion of the information presented in chapter three can be found in the journal article "Metamaterials enable chiral-selective two-photon luminescence from

quantum emitters," as published in *Advanced Materials*.[4] The information presented in chapters two and three were reproduced with permission from Wiley Publishing Group.

CHAPTER I.

Chirality

Just as there exists a ying and a yang, or a good and an evil, the concept of chirality describes the parity of left and right handedness, and its mirror asymmetry. A chiral structure can be identified by acknowledging that its mirror image can never be superposed onto itself.[5] The structures look visually similar, but they are unique and complementary to each other. The original unit structure and its non-superposable are said to be enantiomers of each other. Another term for enantiomers is optical isomers. Just like our hands are chiral structures, organic compounds on the molecular level often exhibit the property of chirality if their structure lacks a point of inversion symmetry (a stereocenter), though this is not a necessary criterion.[6] In the realm of optics, if the structure harbors a subunit that is of a light absorbing nature, the incident light will be transmitted in an asymmetric manner. More specifically, if the absorbing groups within the molecule or structure are arranged in a geometrically chiral manner, the far-field transmission when subjected to either circular polarization of opposite handedness will demonstrate chiroptical properties known as circular

dichroism, CD, and if subjected to a linear polarization, optical rotatory dispersion, ORD.[5, 7] While CD describes the asymmetric absorption of left (LCP) and right (RCP) circularly polarized waves, ORD describes the polarization rotating ability of a material both over a range of wavelengths. ORD should not be confused with optical rotation, which refers specifically to the rotation of the plane of polarization of a linearly polarized beam typically for a given wavelength.[5]

$$CD = T_{RCP} - T_{LCP}$$

ORD can be converted to CD through the Kramer's Kronig relations. The direction of rotation is known as either a dextro- or levo- rotation and identifies whether the enantiomer is dextrorotatory, thereby creating right circularly polarized light, or levorotatory, thereby creating left circularly polarized light when viewed from the detector. Because the chiral object responds differently to the two opposite circular polarizations, which is seen in the different transmission spectra, refractive indices associated with the two polarizations can be used to describe their individual responses. This was first demonstrated by Fresnel in 1825.[5] The classic, optical definition for the orientation of circular polarizations is utilized in this thesis. Here, right circular polarization is seen as clockwise as it propagates towards and is viewed from the detector. Respectively, left circular polarization is seen as rotating counterclockwise as it is viewed from the detector.

Chirality is a useful tool for identification and quantification of chemical species. The manipulation of light by a chiral structure as described above provides an identifier through which to classify that material. By measuring the amount or type of rotation experienced by the light, values of enantiomer concentration can be reached, making chirality a useful tool in industrial and biological applications to identify compounds or measure concentrations.[5] In the past, optical rotation was the go-to measurement for describing the chiral-strength of a molecule, however as technology advanced tools like the photo-elastic modulator eventually became the standard for measuring circular dichroism. There are a few reasons behind this, but a common issue is that rotational measurements of linearly polarized light can overlap, for instance if the material provides greater than a 180° rotation of polarization over the typical 10 cm measuring stage, it is difficult to distinguish if the rotation is α or $\alpha + n \times 180$, where n is an integer. While in natural organic molecules, optical rotation provides values on the level of millidegrees[8] at the sodium line (λ=588, 589 nm), chiral metamaterials can provide values on the order of 100x degree.[9] Often times the values of organic molecules are stated in terms of specific optical rotatory power also known as specific rotation $[\alpha]_{\lambda}^{t^0}$.

1.1Chirality in Nature

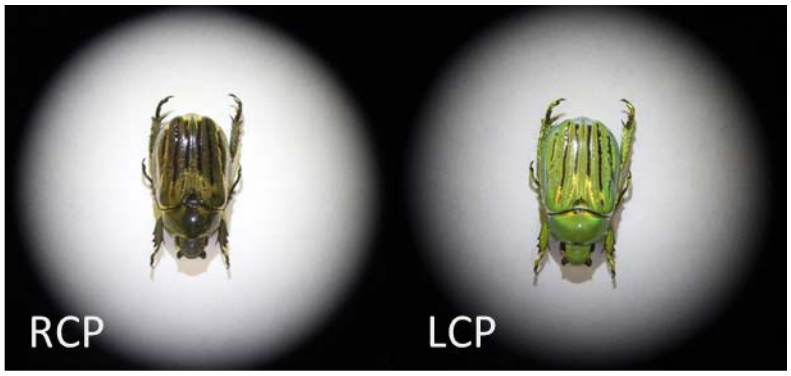

Figure 1.1: Chrysina Gloriosa On the left under an LCP analyzer and on the right under an RCP analyzer.

As previously discussed, chirality is found at the basis of organic structures and nature utilizes it to great lengths in biochemistry in order to achieve a wide variety of effects, be it on the molecular or protein folding level. In 1874 Jacobus Henricus van't Hoff discovered that the tetravalency of the carbon atom could lead to chiral structures. Van't Hoff related the handedness of the chiral atoms to that of optically active crystals of tartaric acid that Pasteur studied. Van't Hoff's objective was to provide "a more definitive statement about the actual positions of the atoms."[10]

In some cases the rotation of a single bond can lead to configurational isomerism, meaning that the chemical composition is identical, however its configuration is slightly shifted to form a different molecule. In biochemistry this

can have huge effects, for instance the rotation of a single bond can change l-glucose to d-glucose. The l-isomer can only be synthesized in a laboratory, and cannot be use an energy source for living organisms. Simple enantiomers have enough dissimilarity such that their difference propagates in the overall structure of the complex macromolecule, potentially achieving a massive net effect simply due to the handedness of the molecule. This feature of chirality on the molecular level provides optical finger prints. When passing light through these chiral objects we are capable of identifying the difference between the two possible structures. However, in nature chiroptical properties are extremely weak. For instance, chirality manifested in the form of optical rotatory dispersion is often used to measure the concentration of a sugar solution. However to accurately quantify this type of rotation from organic molecules, either a large concentration is required in a small cuvette or if you are measuring concentration a large cuvette length of 10cm is required.

Few organisms are thought to demonstrate circularly polarized dependence however the list is consistently growing. For example, the mantis shrimp can produce circular polarizations with its tail and detect the circular polarizations with certain segments of its compound eye.[11] Meanwhile other organisms are currently only known to 'generate' circular polarizations such as the Chrysina

genus of beetles that reflects one circular polarization, but not the other.[12] Figure 1.1 presents this organisms unique feature. The broadband circular reflectance produced by some beetles like the Chrysina aurigans[13] is much like that of a liquid crystal, with the planes of the crystal oriented in a helical fashion. The portion of the exoskeleton that provides the green and brown contrast when analyzed for the two opposite polarizations is said to be cholesteric in nature.[14]

However, the application of chirality in biochemical studies is not limited to the conventional, linear regime. In fact, the realm of biological characterization employs the second-order susceptibility tensor of some biotic matter such as collagen and striated tissues to investigate their structure, shape, deformation and orientation.[15-17] The chiral selectivity of a biological sample's second harmonic response is typically orders of magnitude larger than its counterpart in the linear regime; however the nonlinear response can only be activated in materials that are chiral or non-centrosymmetric. Thus, chiral materials are naturally suited for second-order nonlinear interactions because all chiral structures are intrinsically non-centrosymmetric and therefore possess non-vanishing values of the second order susceptibility $\chi^{(2)}$. For this reason, chiral second harmonic generation (SHG) has been utilized as a powerful tool for

probing the structure of interfaces, organic tissues, and biochemical agents.[9, 18-21]

1.2Chirality in Metamaterials

Despite the aforementioned applications, chiral responses from naturally occurring materials are generally very weak, thereby prompting the development of artificially structured optical media with unusually strong chirality. [7] The past few years have witnessed an explosive development of chiral optical metamaterials that exhibit circular dichroism and optical rotation orders of magnitude larger than conventional materials.[22-31] However chiral metamaterials have been designed for some time. For instance, artificial chirality has been achieved as early 1898 by Acharya Jagadish Chandra Bose. Bose's motivation was to imitate the optical rotation of chiral like structures by using "elements of molecules of twisted jute."[32] Figure 1.2 shows a series of chiral structures that have contributed to the realm of chiral metamaterials. A sufficiently strong chiral effect in metamaterials can also lead to intriguing phenomena such as negative refraction[33, 34] as well as important applications including circular polarizers,[35] beam splitters,[36] and biochemical sensors.[8] A couple good review papers can be found here for chiral metamaterials.[28, 37]

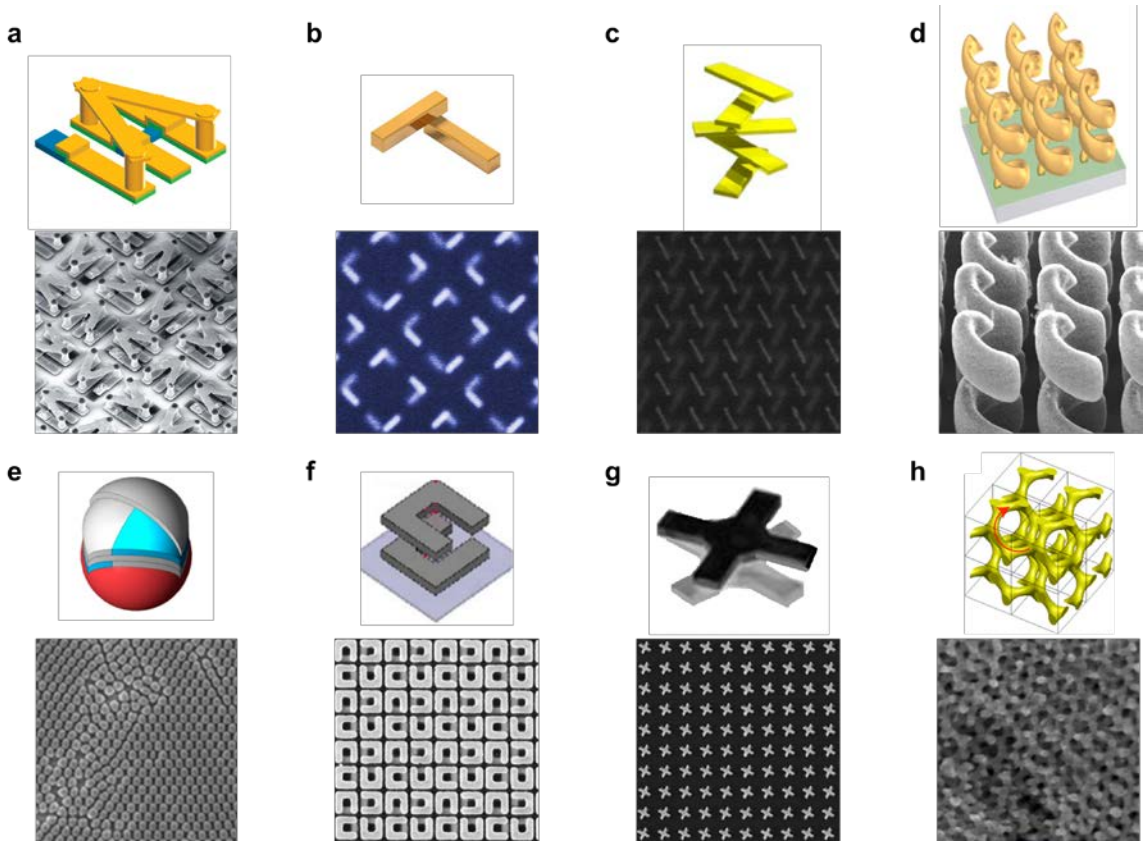

Figure 1.2: Chiral metamaterial structures from the literature. a) Structure used for chiral switching [38] b) Simple bar structure for theoretical modeling [23] c) Stacked chiral bars for a broadband effect[27] d) Helical meta-atoms for continuous modification of the circular polarization as the wave passes through the material [35] e) Self-assembled monolayers for industrial grade chiral responses[39] f) Split ring resonator used as one of the first chiral demonstrations [40] g) twisted cross was used to create heightened chiral, nonlinear responses [41] h) Self assembled block copolymers filled with metal to create a 3D mesh[42]

It should be noted that it is the spatial distribution of the excited states of the species or structure that causes circular dichroism. As the light passes through the structure, the unit must contain absorbing components along the direction of propagation of the incident light. At first many metamaterial papers relied on angular incidence of flat two-dimensional structures in order to generate

chiral responses.[43-45] These resonances were achieved by sculpting the 3D electric field by using the 2D metamaterial at an angled incidence. Over time, the field recognized that overlapping structures along the propagation direction of light was truly necessary, thus creating structures that could manipulate the light as the light passed through the structure at normal incidence.[23, 24, 27, 46] Applying light at normal incidence also helps to remove potential artifacts in measurements such as anisotropy.[28]

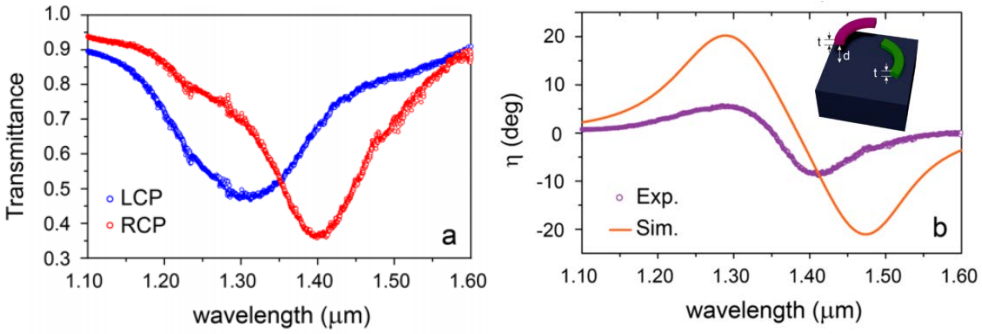

Figure 1.3: Chiral properties of a twisted nanoarc pair in the infrared. (a) Measured transmission spectra of LCP (blue) and RCP (red) light waves at normal incidence. (b) Ellipticity η of transmitted light obtained from experiments (purple) and simulations (orange). The twisted arc metamaterial structure at longer wavelengths displays the cotton effect.[47] Reproduced with permission from Nano Letters.

Utilizing these concepts, our group designed its first chiral metamaterial. The published research describes a pair of arcs twisted in the k-direction (propagating direction of light) that demonstrates large circular dichroism and optical rotation in the infrared regime.[17] Figure 1.3 provides some of the

crucial findings of the papers and illustrates for us the twisted arc structure. The 3D structure of the chiral metal arcs are capable of producing a chiral response at normal incidence. The chiral nature of the structure is demonstrated by the cotton effect, which describes the coincidence of optical rotatory dispersion and the circular dichroism at the same spectral location.[5] This effect is witnessed in Figure 1.3 where the elliptical maximum, circular dichroism maximum and the optical rotatory dispersion inflection point occur at roughly the same wavelength of 1.35μm. The results from this twisted arc structure become a crucial starting point for my own research, which is presented in Chapter 2.

Chirality has opportunities to pour its properties into a wide range of optical methodologies, techniques and applications. The next subsection will discuss the origin of chirality in metamaterials. The following subsections will describe how chiral metamaterials are being used to achieve unexpected optical phenomena, or achieve optical traits of structures using chiral materials. The future of chirality in artificial structures will require the manipulation of the chiral signals, whether it's with reconfigurable materials, voltage biasing, or optical pump-probe techniques.

1.2.1 Origin of Chirality in Metamaterials

With regards to chemical species, the origin of the circular dichroic behavior can be traced back to a section of the chiral molecule known as a chromophore, which absorbs the impinging light. The chromophore or chromophores within the molecule absorb the light and stabilize the excited state along the rest of the structure. This same property can also explain how chiral metamaterials achieve their circular dichroic properties. In this case, however, the absorption of light is typically due to a resonance feature within the material. The theoretical understanding behind the absorptive resonance of these metamaterial structures can be described by the Born-Kuhn model. This model, as an offshoot to the Drude-Lorentz model, utilizes two charged particles that are coupled to each other. Depending on the resonance of the coupled particles, one can imagine how a linearly polarized beam passing through these charged particles, might rotate the incident wave.[23, 48] As described by Rogacheva and Yin, the coupling of the particles leads to two excited states, one called the bonding and the other the antibonding state, each with their own distinct energy levels. The excited state corresponds to the increased absorption witnessed during a circular dichroism measurement. This is witnessed in our groups first chiral metamaterial as seen in Figure 1.4.

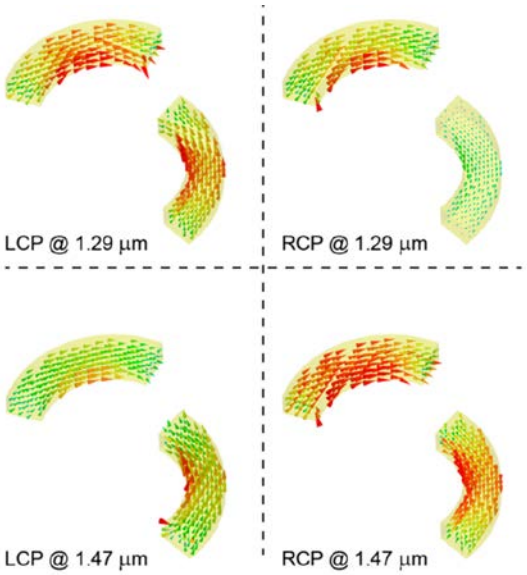

Figure 1.4: Chiral nanoarc pair in the infrared showing bonding and antibonding states for the resonant wavelengths of 1.29 and 1.47 µm as seen in Figure 1.3.[47] LCP at 1.29 µm and RCP at 1.47 µm are the resonant polarizations at their respective wavelengths, thus showing enhanced electric fields. Reproduced with permission from Nano Letters.

1.2.2 Negative Refraction

What first brought chiral structures their spotlight in the metamaterial research field was their ability to create negative refraction. Achieving a negative refractive index implies that both the electric permittivity and the magnetic permeability of a given material must both be negative. This was one of the first goals of metamaterials, as negative refractive materials are not found in nature. Although 2D split ring resonators were the primary structure to enable and demonstrate this property[49], it was later realized that chiral structures could

provide an alternative route to generating negative refraction. To date, this subset of chiral metamaterials has been prolifically researched and chiral metamaterials with negative refraction have been demonstrated in the optical[50], terahertz[34] and microwave regimes[48, 51].

1.2.3 Giant Chiral Signals

It was quickly realized that the effects of chiral metamaterials could be significantly enhanced and used to create giant chiral properties. The two quantities measured that distinguish the highly chiral effects of metamaterials are circular dichroism and optical rotation. The progression from planar structures with large unit cells to bilayered structures with slight twists in the two layers to using fully isotropic materials has made an enormous increase in the effect of the signals. To achieve high circular dichroic responses it is essential to manipulate the unit cell structure in the direction relative to the propagation of incident light. This k-direction manipulation provides the light absorbing necessary as the circularly polarized wave passes through the material. Knowing the pitch of the impinging wave, the spacing between bi-layered or multi-layered structures and the angle of twist induced in each plane of the structure is absolutely essential to creating the ideal chiral metamaterial.

Fabrication of such chiral structures can be achieved in a multitude of ways, many of these methods can be seen in Figure 1.2. For instance, Figure 1.2h uses polymer scaffolding to create 3D metamaterial structures. In addition, Figure 1.2d utilized laser ablation to create helical metamaterials in the infrared. In an attempt to produce these large chiral effects on an industrial level one group has used self-assembled micron-sized spheres in conjunction with glanced angle deposition to create a 3D chiral effect, as seen in Figure 1.2e. Chiral photonic metamaterials, nanoscale-engineered metal-dielectric materials, provide distinctions of optical chiral responses that surpass naturally occurring materials by many orders of magnitude.[22, 24, 27, 28, 30, 35, 41, 47, 52-55] Their applications offer potential for enhanced enantio-selectivity in the biological[8], industrial[56] and photonic industries.[33, 57]

1.2.4 Nonlinear Chiral Responses

Despite the massive increase in circularly dichroic responses from metamaterials in the linear regime, the field pushed further to seek out other methods to provide enhanced optical activity. The nonlinear counterparts of circular dichroism and optical rotation exhibit heightened responses to their

linear versions. The more pronounced responses are due to the nature of chiral metamaterials. That is, chirality and nonlinear responses require a similar property in order to achieve either effect : a lack of symmetry. Spatial symmetry or a lack there of can have an impact not only on linear electromagnetic effects but also on their nonlinear counterparts. For instance, chiral point groups 1, 2, 3, 4, 6, 222, 422, 622, 32, 23, 432 are also noncentrosymmetric point groups. A centrosymmetric material is one that holds a center of symmetry, this center of symmetry nullifies the second order susceptibility terms.[58] Therefore when a material is noncentrosymmetric, the likelihood of generating a nonlinear response within that material is significantly higher. Specifically noncentrosymmetric materials can give rise to second order optical nonlinearities.

The induced polarization of a beam incident on a material can be attributed to the linear susceptibility $\boldsymbol{P} = \chi^{(1)} \cdot \boldsymbol{E}$. As mentioned, when impinging high intensity beams, the nonlinear susceptibility can be induced. The induced polarization of these higher order fields is characterized by the nonlinear susceptibility tensors $\chi^{(2)}$ and $\chi^{(3)}$ and is described by[59]:

$$\boldsymbol{P} = \chi^{(1)} \cdot \boldsymbol{E} + \chi^{(2)} : \boldsymbol{EE} + \chi^{(3)} \vdots \boldsymbol{EEE}$$

The second harmonic term is often the largest of these values. If an external field is applied the $\chi^{(3)}$ can be used to generate electric field induced second harmonic generation (EFISH).[60] The second order nonlinear susceptibility is a third rank

tensor.[58] Within this tensor there is a possibility for chiral materials to have a term $\chi_{xyz} = -\chi_{yxz}$. This term is in part responsible for the intensified chiral responses seen in second harmonic generation-circular dichroism (SHG-CD).

However, the nonlinear behavior of chiral metamaterials with intensity-sensitive optical properties or wave mixing characteristics, has thus far received rather scant attention. Of the previous nonlinear, chiral studies, the topics have focused on single meta-atom imaging and refinement of minor structural deformations that contribute to extreme hot spots.[46, 52, 61, 62] In addition, these studies apply SHG imaging to further understand metamaterial resonances and field enhancements in the chiral structures. The limited but essential research in this field demonstrates that nonlinear, chiral metamaterials offer significant potential for three major reasons. First, just as SHG requires the disruption of symmetry in order to produce a non-centrosymmetric $\chi^{(2)}$ electromagnetic tensor, a unit cell must not have a point of inversion symmetry in order to produce chirality. By disrupting the typical symmetry for the susceptibility tensor, the harmonic response is forced to rely on the handedness of the structure, thereby allowing for disambiguation of the two enantiomers in the nonlinear regime. Secondly, metamaterials consisting of metallic particles of subwavelength dimensions have pronounced optical resonances which magnify

their SHG response. These optical responses spawn from the properties of the metallic nanoparticles, including localized surface plasmon resonances, lightning rod effects, and their high surface to volume ratio. A third reason to explore nonlinear responses for chiral metamaterials is that metals offer the perfect platform by which to induce surface-second harmonic generation. This type of SHG is most strongly witnessed at interfaces where the symmetry of a material's electromagnetic tensor $\chi^{(2)}$ is disrupted due to the juxtaposition of another material at that interface. For these reasons, nonlinear responses in chiral metamaterials show enhanced contrast between oppositely circularly polarized waves. The study of nonlinear phenomena in chiral metamaterials is also in-line with the emerging field of nonlinear metamaterials, which promises exciting opportunities to create customized nonlinear media with artificial, molecular arrangements and tailored geometries.[63-66]

The addition of these advanced techniques has provided enhanced enantiomer selective microscopy and strengthened the identification of optically active structures, however the overall chiral distinctive properties of naturally occurring materials remain weak and are mostly limited to the ultraviolet spectrum. In this way, the realm of metamaterials provides the opportunity to build upon the existing platform of chiral handedness that nature has offered.

1.2.5 Extreme Signal Properties

Chiral metamaterials have been utilized to achieve several other properties that are limited to that of meta-structured materials. For instance, metamaterials are capable of obtaining strong resonances. When the materials are engineered in a certain fashion, they can create perfect absorption over a certain wavelength range.[67] This perfect absorption technique shows strong promise for future radar technologies.

Chiral mirrors are an interesting topic that has surfaced earlier this year (2015). To understand chiral mirrors first we must understand how a normal mirror interacts with circularly polarized light. For instance, when light is incident on the surface of a silver mirror, which is highly reflective for both TE & TM polarizations in the visible regime, the electromagnetic waves simply inverts its propagation direction, thereby inverting LCP light to RCP light. This can be further understood by looking at Jones calculus for a normally incident circular polarized wave on a perfect mirror. With the use of chiral metamaterials however, LCP light incident on the chiral surface can be maintained as LCP light as it is reflected at normal incidence.[68] Other potential features of chiral mirrors include perfect absorption. For instance, these structures could near perfectly reflect one of the two circular polarizations while absorbing the other. Similar features can be achieved in cholesteric liquid crystals[69] or with oriented thin polymer films. A typical property of chiral mirrors is to either absorb at a

specific wavelength for one circular polarization while reflecting a broadband spectrum for the other. However, it has been show that it is possible to reflect one spectrum over a broadband spectrum while absorbing the other.

The last extreme property to be mentioned here is that of super chiral fields in chiral plasmonic structures. The helical pitch of the circularly polarized illumination can be compressed such that its pitch matches that of a material's twist, thusly creating a superchiral field.[70]

1.2.6 Chirality for Biosensing

Perhaps the holy grail of chiral metamaterials at one point was to achieve the ability to place a chiral molecule in the presence of a metamaterial structure and enhance the field to such a degree that any molecule could be detected with its own chiral footprint. While one paper has shown progress towards this goal[8], the ability to sense chiral signals with chiral metamaterials appears to be a feat still left to accomplish. A great deal of research regarding single atom sensing was immediately published at the surge of nano-plasmonic materials in the early 2000's, however the majority of these works don't focus on enhancing chiral signals[71-73] and the one's that do, struggle with extracting the pertinent chiral sensitive information. In addition, chiral nanoparticles on the level of $<$5nm also show chiral features themselves as they cannot obtain their full bulk properties, thus complicating the distinction between the two.[28]

1.2.7 Filling the Gap

In order to push the ability of chiral metamaterials further, this thesis investigates how chiral metamaterials will react under nonlinear excitation conditions. An initial focus on enhancing signals from chiral media was determined. By first modifying the design provided by Cui et.al in the infrared regime a chiral metamaterial in the visible regime was created. The material composed of two bilayered, nano-arcs showed outstanding visible responses.

To further the contrast between the chiral responses, nonlinear enhancement of the signals was targeted. As mentioned earlier, a small set of research has been demonstrated on nonlinear signal generation or wave mixing in chiral metamaterials. Of the existing sources, many showed extreme hot spots or low nonlinear circular dichroic results. For this reason, experimental research was provided by utilizing the same nanoarcs mentioned to enhance the linear response in the visible regime.

A second initiative was to find a way to extract this enhanced nonlinear effect. As will be seen, simulations of the chiral arc in the linear regime demonstrate hot spots within the dielectric material surrounding the silver nano-arcs. As these hot spots appear at resonantly circular dichroic locations, there exists potential to extract this enhanced contrast. The initiative of this work was

to utilize quantum emitters, or quantum dots, to absorb this intensified signal and extract it through an emission signal. This method goes beyond the typical reflection, transmission, absorption measurements used in chiral metamaterial research. The extracted results showed outstanding enhancement of the linear regimes chiral contrast.

CHAPTER II.

Nonlinear Imaging and Spectroscopy of Chiral Metamaterials

Chirality is most commonly identified with linear optical characterization techniques, however opposing circularly polarized waves can also display the same parity as a property of higher order optics. Here, a chiral metamaterial is presented that produces both distinguishable linear and nonlinear resonant features when probed with left and right circularly polarized incident beams in the visible to near-infrared regime. The material demonstrates a linear transmission contrast of 0.5 between left and right circular polarizations and a 20× contrast between second harmonic responses from the two incident polarizations. Nonlinear and linear response images probed with circularly polarized lights show strongly defined contrast.

2.1 Design & Simulation

This effort presents a number of noticeable features that favor a comprehensive study of chiral-selective nonlinear processes in metamaterials. Our sample possesses engineered structural variation along the propagation direction, which enables strong chiral responses for transmitted light at normal incidence. The size of the unit cell is substantially smaller than the wavelength of light under consideration, which allows us to treat the chiral periodic structure as a metamaterial and describe its properties using homogenized parameters. Spectral-resolved circular dichroism of both linear and harmonic signals are analyzed, compared, and utilized for imaging of a chiral pattern consisting of both enantiomers.

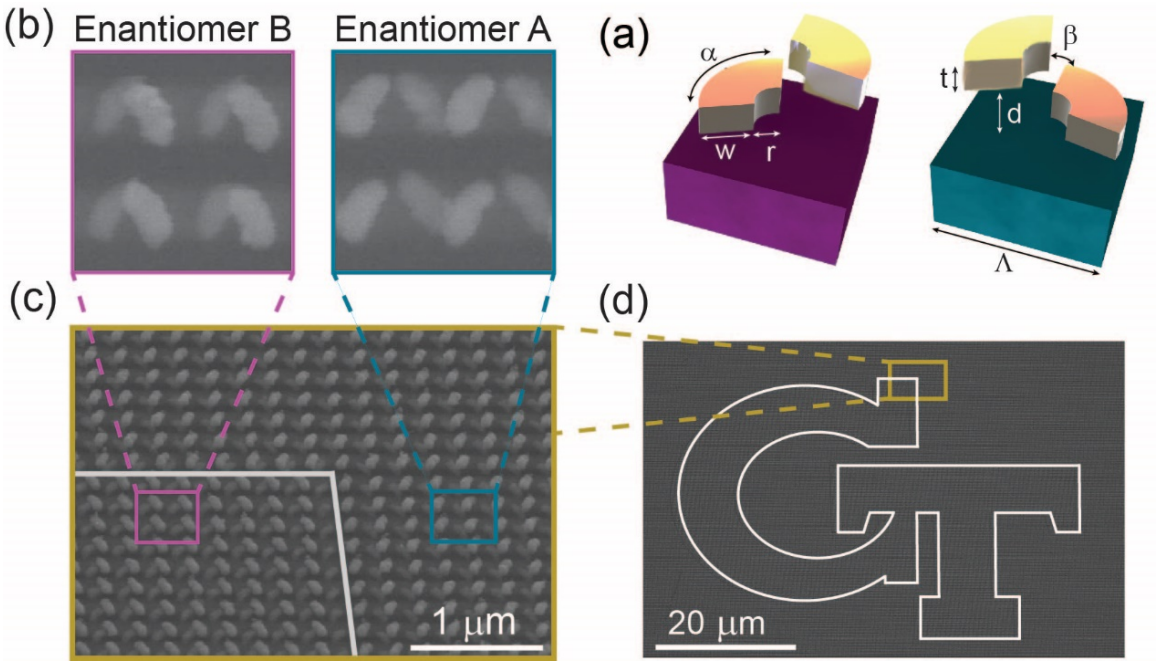

Figure 2.1: Design and simulation of the metamaterial pattern consisting of twisted arcs of both enantiomers. (a) Schematic of chiral enantiomer A (right) and B (left). Structural parameters were optimized via rigorous full-wave simulations: d=72 nm, t=42 nm, w=70 nm, r=32 nm, Λ=225 nm, α=90°, β=15°. (b) An SEM image of the enantiomers A and B, where the upper chiral arc is more visible and thus has a lighter color in the image. (c) A tilted view of a corner of the patterned 'GT' logo, where a white line is shown to distinguish where the two enantiomer structures meet. (d) An SEM image of the patterned 'GT' logo. Here, the inner region of the logo hosts the B enantiomer and the outer region hosts the A enantiomer.

The chiral metamaterial in this research is based on a twisted-arc structure, which has been employed previously to realize artificial chirality in the infrared frequency ranges.[47, 74] Using optimized parameters along with a multilevel aligned lithography technique, we are able to downscale the previous design and obtain a giant chiral response near the red end of the visible spectrum. The metamaterial pattern, 100×100 μm^2 in size with roughly 10^5 arc

pairs, implemented both enantiomers A and B (see Figure 2.1a) into a pattern to create the Georgia Tech "GT" logo. Figure 2.1,b-d shows the scanning electron microscope images of the sample at a series of magnifications, from the single meta-atom level to the entire pattern. Due to limitations produced by our lithography alignment system a 15 nm longitudinal shift occurred between our upper and lower chiral arc pairs, however the lateral alignment remained ideal.

2.2 Fabrication process

Electron beam lithography was used to create a bi-layered metamaterial with parameters specified in Figure 2.1a. To create this multi-staged material, a series of steps involving PMMA coverage, lithography, etching and silver layer deposition were applied. The full fabrication workflow can be seen in Figure 2.2.

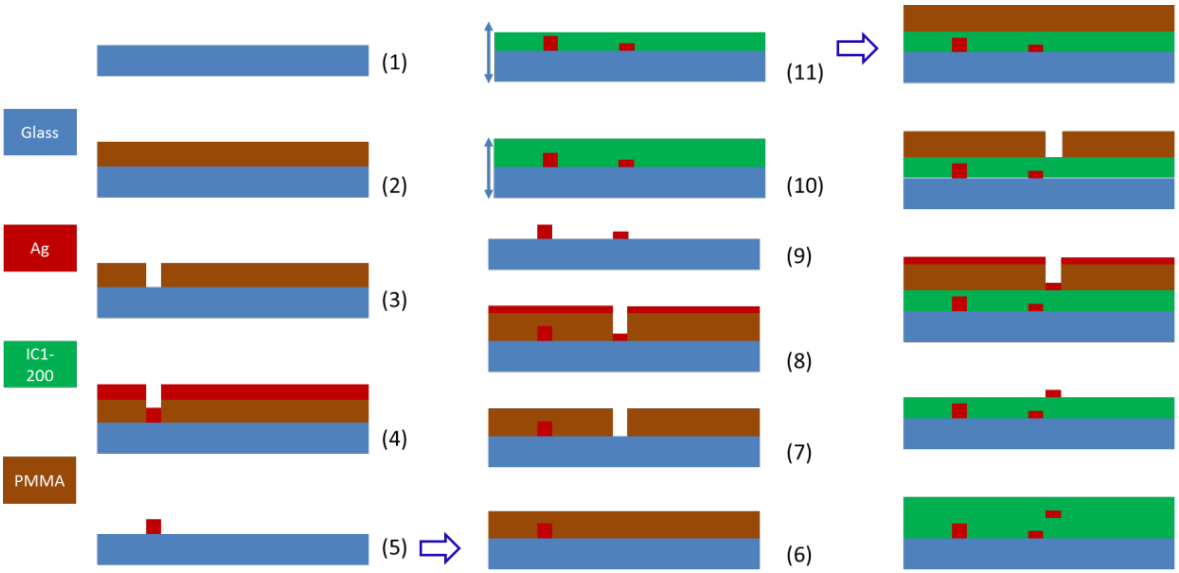

Figure 2.2. Fabrication flowchart of the twisted-arc photonic metamaterial.

The fabrication listed here is similar to that of a previous paper demonstrated in our research group, with a critical extra step of plasma etching of the first layer of spin on glass.[47] The fabrication of the twisted-arc photonic metamaterial primarily includes three runs of aligned electron beam lithography. The fabrication flowchart illustrated in Figure 2.2 includes the number processes indicating the sequential steps taken. The metamaterial was fabricated on a 1×1 inch^2 clean glass substrate (1). The first run of electron beam lithography was to define the alignment marks necessary for the later steps. Electron beam resist polymethyl methacrylate (PMMA) A7 of 800 nm in thickness was spin coated at 1000 rpm with 2 seconds of ramping time for 60 seconds (2). The PMMA resist was prebaked at 180 °C for 90 seconds. After that, to eliminate the charging

effect on the dielectric substrate during the electron beam patterning, another layer of water soluble conductive polymer Espacer 300z was spin coated at 2000 rpm with 1 second ramping time for 30 seconds. Next, electron beam lithography (JEOL JBX-9300FS EBL) was carried out to define the alignment marks. After rinsing the Espacer 300z with deionized (DI) water, the PMMA resist was developed in the mixture of isopropyl alcohol (IPA) and Methyl Isobutyl Ketone (MiBK) with a volume ratio of 1:1 for 2 minutes (3). Afterwards, a 10 nm thick titanium and 200 nm silver layer were deposited by electron-beam evaporation (4). Subsequently, a lift-off process using acetone solution was carried out to finish the patterning of the alignment marks (5). The second run of the aligned electron beam lithography was carried out based on the predefined alignment marks. PMMA A4 was spin coated with 4000 rpm and 2 seconds ramping time for 60 seconds (6). After pre-baking the PMMA resist at 180 °C for 90 seconds, the Espacer 300z was coated in the same procedure as step (3). After that, aligned electron beam lithography was used to define the pattern of the bottom layer of the arc array, followed by the removal of the Espacer 300 and the development of the PMMA (7). The bottom layer of the silver arcs was then formed by electron beam evaporation of 50 nm thick silver (8) and a lift-off process (9). On the top of this silver structural layer, a transparent dielectric

IC1-200 (Futurrex Inc.) was spin coated at 5000 rpm with 2 seconds ramping time for 60 seconds (10), and then heated at 200 °C for 60 seconds to remove the solvents. Afterwards, the dielectric was then plasma etched to form a flat dielectric platform of 70 nm just above the substrate, for the subsequent patterning of the upper metallic layer. Finally, for the third run of aligned electron beam lithography, exactly the same procedures (12- 15) were repeated to form the top silver arc array of the metamaterial. After that, to reach the targeted performance and protect the sample from degradation, additional spin coating of the IC1-200 followed by baking were performed to form a transparent top cladding of 1.1 μm in thickness (16), and the fabrication of the twisted-arc chiral metamaterial was accomplished.

2.3 Linear Response

The twisted-arcs are expected to interact differently to circularly polarized lights of opposite handedness, as indicated by the simulated transmission spectra of enantiomer A in Figure 2.3.

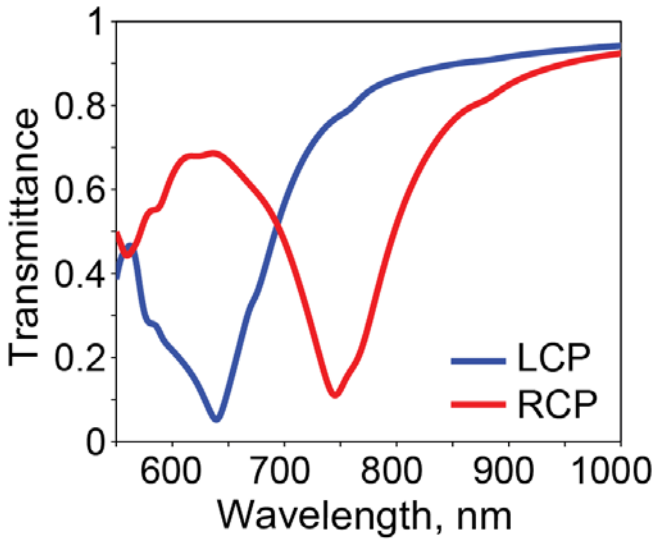

Figure 2.3: Simulated transmission spectra of enantiomer A under LCP illumination and RCP illumination with dips at 640 and 750 nm respectively.

The chiral response of a material is typically measured by the parameter of circular dichroism (CD), which is most commonly treated as the difference in extinction of left-circularly polarized (LCP) and right-circularly polarized (RCP) waves: $CD = T(\omega)_{RCP} - T(\omega)_{LCP}$. The phenomenon of absorbing different polarizations of light is conventionally due to a chiral chromophore, or light absorbing group that is found in organic substances. In contrast, our metamaterial provides its light absorbing to create its chirality by forming a resonance, between two metallic structures, that is sensitive to the angular momentum of impinging photons.

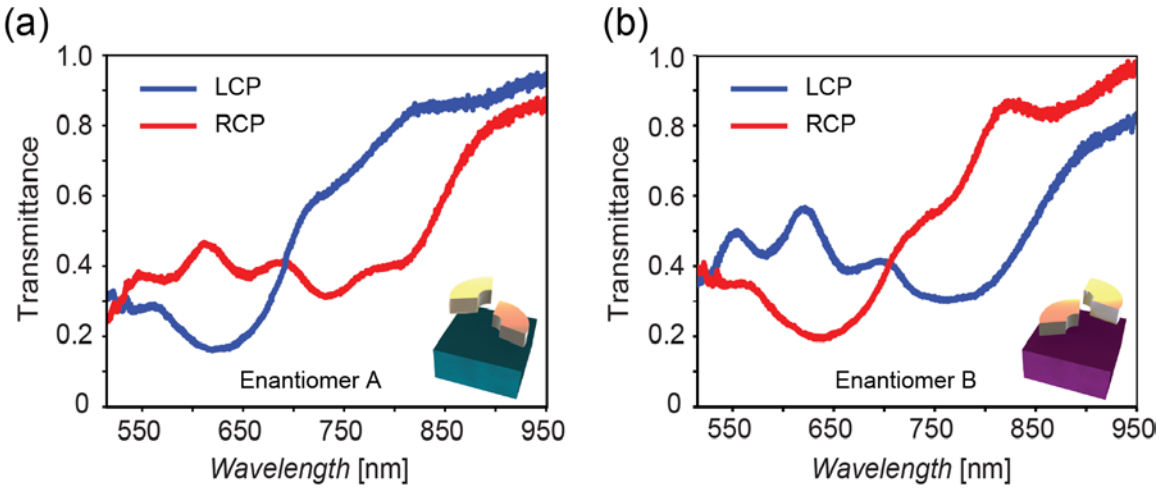

Figure 2.4: Linear spectroscopy (a) Transmission spectra of enantiomer A for circularly polarized lights. The spectral location of the resonance is sensitive to the handedness of the incident states of circular polarization. A contrast of ~ 3dB in transmission is observed around the resonance frequencies. (b) Transmission spectra of enantiomer B, which are completely complementary to those of enantiomer A.

Figure 2.4,a-b shows the transmission spectra of the two enantiomers excited with both LCP and RCP waves, which were obtained using broadband circularly polarized light at normal incidence. Defined resonance dips for enantiomer A are seen at wavelengths of 625 nm and 740 nm for LCP and RCP waves respectively. These spectra are completely complementary to those for enantiomer B with corresponding dips at similar wavelengths. These measurements correlate well with the numerical results shown in Figure 2.3, although the measured resonances appear broader and shallower than the simulated ones due to fabrication uncertainties and size distribution in the actual sample. Around these defined resonance dips, our chiral arc pairs demonstrate

strong chiral, optical activity in the visible and near-infrared regime. The difference in spectral location of resonance under circularly polarized illumination of opposite handedness can be further explained by the Born –Kuhn model.[23] In general, our meta-atomic structure undergoes an interaction that causes the two chiral arcs to resonate reciprocally at wavelengths of 625 nm and 740 nm for the two enantiomers. The circularly polarized, incident beams are intensity-reduced by the resonances of the specific enantiomer, thereby creating circular dichroism. Figure 2.5 demonstrates the circular dichroism of the enantiomer pair, which was obtained by taking the difference of the transmission curves in Figure 2.4,a-b respectively. The CD effect is maximized near resonance dips in the transmission spectra, producing a maximal magnitude of approximately 0.5. The CD curves of the two enantiomers are again complementary, thereby appearing as mirror images of each other with respect to the horizontal axis of CD = 0.

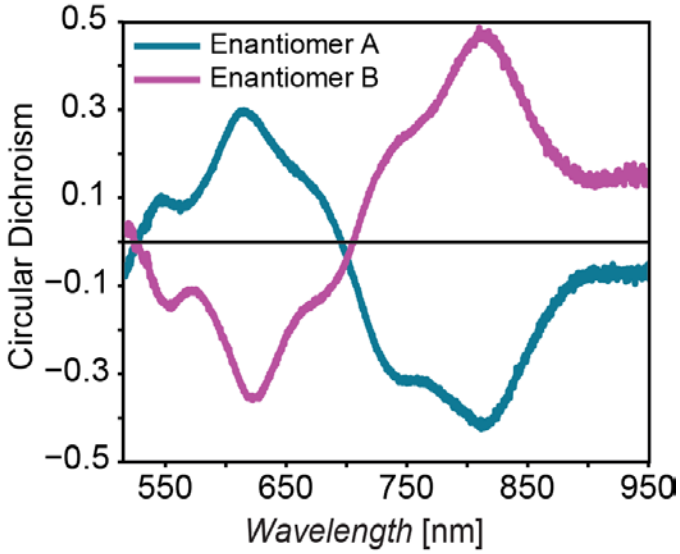

Figure 2.5: Circular dichroic response from the enantiomer pair, CD = $T_{\mathrm{RCP}} - T_{\mathrm{LCP}}$. The CD effect is maximized near resonance dips in the transmission spectra.

2.4 Optical Characterization

LCP and RCP waves are produced from a broadband source followed by a series of optics that create circular polarization. The circularly polarized waves are then incident upon our sample and recorded on a silicon detector. Nonlinear spectroscopy was performed using a Mai Tai laser and a set of appropriately positioned objectives to transmit and collect the incident radiation on the sample. In order to determine the polarization of the nonlinear light emitted from the sample, a series of optics were used to determine the Stokes vectors.

A schematic of the linear optical characterization setup is shown in Figure 2.6. To illuminate the sample a broadband tungsten halogen source (B&W Tek BPS120, spectral range 350-2600 nm) is passed through a coupled fiber that illuminates the rest of the optical path. The light passes through a linear polarizer then a quarter wave plate to create the left and right circularly polarized light. The light is then transformed with a lens, L1 (f = 100mm), and is incident upon the sample. The objective (Mitutoyo, 20× Plan Apo NIR infinity-corrected) then magnifies the region of interest and an iris samples the location of the target sample in the transmitted image. Another lens is again used to transmit the image to the detector. A flip mirror (M1) is shown after the lens. When the mirror is engaged it can redirect the light to help us select which target sample we are looking for via the preceding lens and camera. When the mirror is disengaged the image is sent to a second linear polarizer and a set of 2 filters that cut off wavelengths at 550 and 1000nm. The linear polarizer was used to decompose the circularly polarized light into both a horizontal and vertical polarization with respect to the grating within the spectrometer. From this data, the transmission was calculated by normalizing with respect to the transmission from the substrate.

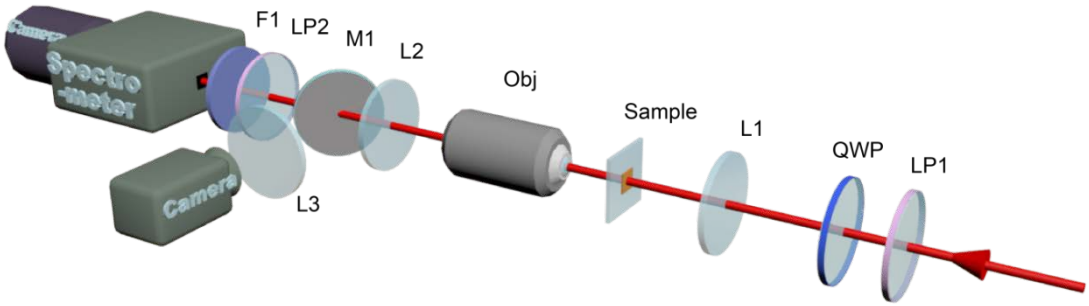

Figure 2.6: Linear transmission optical setup. Abbreviations for optical components: LP – linear polarizer; QWP – quarter waveplate; L – lens; Obj – objective lens; M – mirror; F – filter.

Next, we investigate the nonlinear spectroscopic properties of a chiral metamaterial, and exploit the resonance-enhanced and chiral-selective nonlinear signals for high-contrast second-harmonic optical imaging.

2.5 Second Harmonic Response

While our metamaterial exhibits significant first order chiral selective responsivity, its expected nonlinear optical activity from its second harmonic response will be factors of magnitude larger. For this reason, second harmonic imaging and spectroscopy with chiroptical illumination was performed. All nonlinear measurements in this study were implemented under normal incidence, below the perceived damage threshold of the sample. We also confirmed that no detectable nonlinear signal emerged from the glass and polymer coating or un-

patterned metal films under a similar excitation condition. We first carried out nonlinear spectroscopy measurements on enantiomer A with circularly polarized excitation of constant intensity, as illustrated in Figure 2.7,a-b.

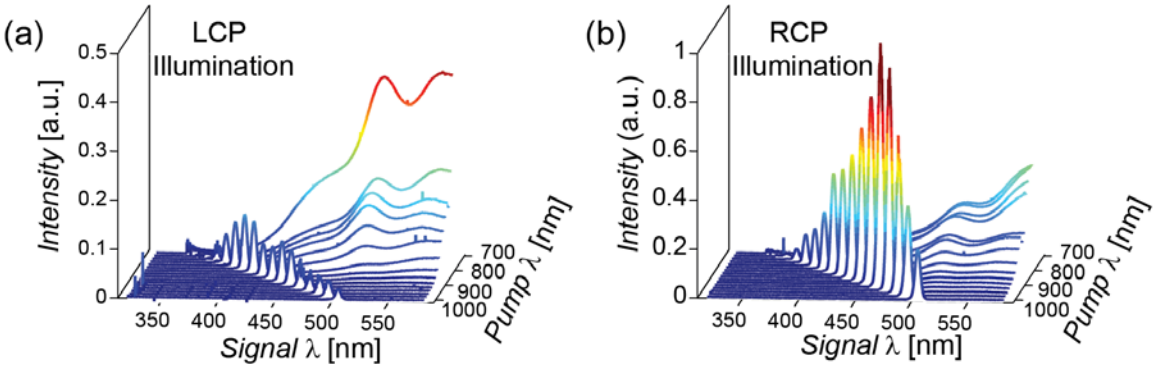

Figure 2.7: Nonlinear spectral measurements of enantiomer A. (a-b) Nonlinear signals from enantiomer A excited by (a) LCP and (b) RCP pump lights. Second harmonic peaks at half fundamental wavelength of the incident light are shown. The LCP induced second harmonic signals are roughly 15% of the maximum RCP induced second harmonic signals. Two-photon luminescence tails are shown trailing off at longer wavelengths of both LCP and RCP induced beams.

Each of the spectral curves features a frequency-doubled peak at half the excitation wavelength, situated on a broadband-background of two-photon luminescence (TPL) trailing off at lower energy wavelengths. The TPL tails are minimized as we near higher excitation wavelengths because less interaction exists between impinging photons and the interband transition of silver. The level of SHG is clearly sensitive to the handedness of the circularly polarized pump light. Specifically, LCP incident light demonstrates a weaker second harmonic signal, less than 10% of the RCP induced response. In contrast,

spectroscopy of enantiomer B will exhibit (not shown) a large second harmonic peak upon LCP illumination in contrast with the RCP induced signal. We also note that the spectral peak of the nonlinear responses were heavily red shifted compared to the linear resonance frequencies. The nonlinear resonance peak can be influenced by the local field enhancement and energy dissipation in the metal, but the SHG signal relies on more complicated factors including the local symmetry-breaking, the vector components of fields, and the outcoupling efficiency at the frequency of the generated wave. This red shift has been observed in other metal based nonlinear plasmonic systems.[75]

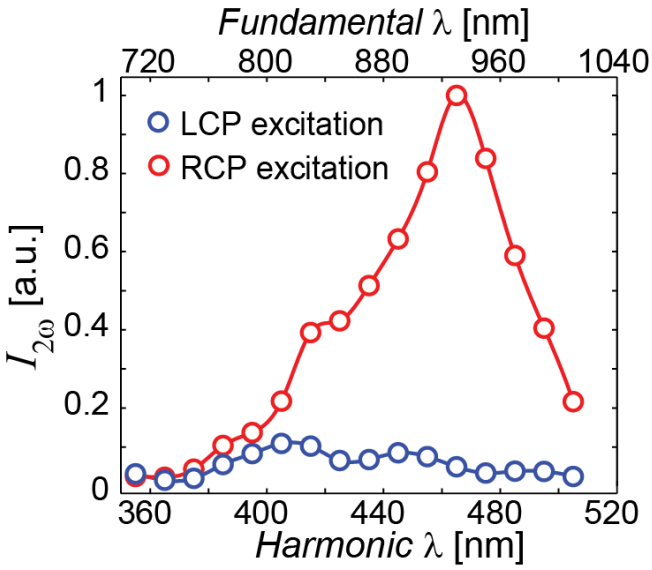

Figure 2.8: Second harmonic response from enantiomer A under circularly polarized pump lights. The peak SHG contrast occurs at $\lambda_\omega = 940$ nm, at which the conversion efficiency of SHG with RCP excitation is over 20 times higher than that of LCP excitation.

Based on the integration of photon counts for the SHG peaks in Figure 2.7 a-b, we obtain the SHG excitation spectra of both enantiomers under circularly polarized pumped beams, as shown in Figure 2.8. A contrast of 20× in the SHG signal was observed at $\lambda_\omega \approx 930$ nm between LCP and RCP beams incident on enantiomer A. This unusually strong contrast, between the two circular polarizations, in the second harmonic spectroscopy in comparison to the linear spectroscopy makes nonlinear measurements an ideal candidate for the detection and imaging of chiral nanostructures.

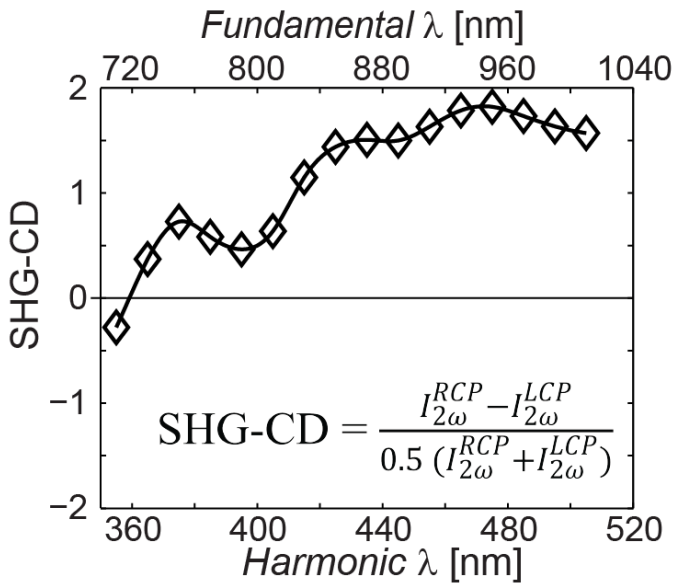

Figure 2.9: Second harmonic circular dichroism of enantiomer A. According to the definition, the maximum possible range of SHG-CD is between the values of –2 and 2.

The harmonic optical activity can be quantified using the SHG circular dichroism, defined as SHG-CD $= \frac{I_{2\omega}^{RCP} - I_{2\omega}^{LCP}}{0.5\,(I_{2\omega}^{RCP} + I_{2\omega}^{LCP})}$. From this definition, the SHG-CD is limited within the range between –2 and +2, and a magnitude of 2 represents an infinitely large contrast in the SHG conversion efficiency between the two incident circular polarizations. Based on the data found in Figure 2.8, we plot in Figure 2.9 the SHG-CD of the chiral-arc pair metamaterial, which indicated an incredibly strong second harmonic circular dichroism of –1.85 at the wavelength of peak contrast.

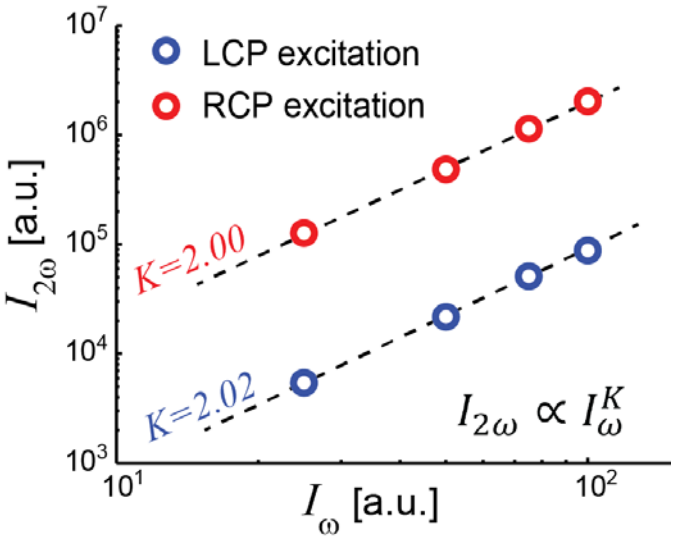

Figure 2.10: The SHG generation dependence on pump intensity, with blue and red markers representing SHG levels under LCP and RCP illumination, respectively. The dashed lines represent fitted curves that display a near-perfect quadratic relation relative to the incident intensity.

We also measured the dependence of SHG signals on the intensity of the circularly polarized pump lights, as shown in the log-log plot in Figure 2.10. As expected, both the LCP and RCP illuminated samples demonstrated a quadratic dependency of $I_{2\omega} \propto I_{\omega}^{K}$, where the exponential factors K_{LCP}=2.02 and K_{RCP}=2.00 are obtained from the least square fitting.

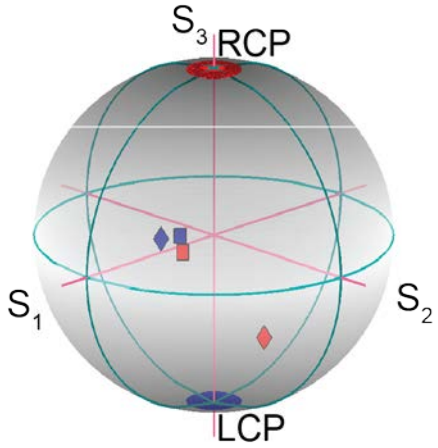

Figure 2.11: Stokes parameters of the outgoing nonlinear waves are plotted on a Poincare sphere from enantiomer A. The diamonds represent induced beams at the peak SHG wavelength of 950 nm, while the squares represent 810 nm where the chiral selective response is less distinguishable. The blue and red marker-fills follow the theme of the paper in representing LCP or RCP induced illumination.

To gain a better understanding of the properties of the second harmonic signal, Stokes polarimetry measurements for enantiomer A were performed at excitation wavelengths of 810 nm and 950 nm for both LCP and RCP waves, and are plotted on a Poincare sphere in Figure 2.11. The interpretation of the Stokes polarimetry measurements assessed can be furthered by calculating the degree of polarization (DOP), the degree of linear polarization (DOLP), and the degree of circular polarization (DOCP) of each second harmonic response which are all normalized to a value of 1. The nonlinear response induced via the RCP beam at 950 nm, where the SHG efficiency peaks, was mostly linearly polarized with a DOLP of 0.90, while all nonlinear responses showed roughly 0.5 for their DOLP.

A consistent microscopic theory of the nonlinear response of this chiral metamaterial would be desirable, but is beyond the scope of this work.

2.6 Imaging

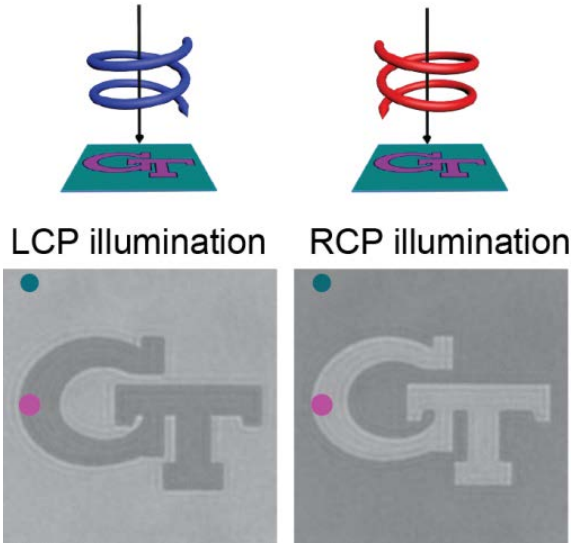

Figure 2.12: The transmission images of the GT sample illuminated with LCP and RCP waves, respectively. The cyan and magenta colored dots placed within the optical images of the sample demonstrate where enantiomers A and B are located.

Figure 2.12 depicts two linear images of the 'GT' patterned logo with different incident, circular polarizations. The images were taken in transmission mode with broadband illumination at a wavelength above 715 nm. The contrast between the two enantiomers is roughly 0.5. As mentioned in Figure 2.1d, the 'GT' pattern is composed of enantiomer A on the exterior of the logo and enantiomer B on the interior of the logo. The transmission spectra observed in

Figure 2.4,a-b elucidates why the interior of the image is dark and the exterior is bright when illuminated with LCP light, as the transmission is higher for enantiomer A than it is for enantiomer B. The same reasoning explains why an inverted image is produced when RCP illumination is shown on the GT patterned sample.

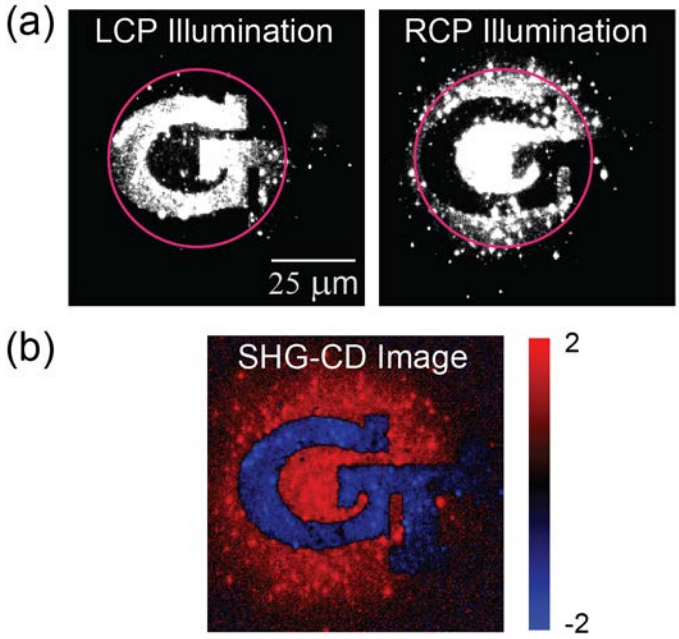

Figure 2.13: Nonlinear imaging. (a) Two nonlinear images of the 'GT' patterned logo are created via high intensity, excitation of RCP and LCP circularly polarized beams. (b) A point by point calculation of the SHG-CD was applied to create the image of the metamaterial pattern shown. Counts recovered from both RCP and LCP illumination displayed in Fig. 2.13a were used to create this image.

Based on these measurements, we then probe the patterned 'GT' logo at a fundamental wavelength of 950 nm, at which the peak SHG-CD was obtained as

seen in Figure 2.8 and 2.9. The second harmonic images of the sample under circularly polarized excitation lights are depicted in Figure 2.13a. The two enantiomers exhibit opposite SHG conversion efficiency, which corresponds to their chiral selective nature as evidenced from the inverted image polarity in Figure 2.13a. The hotspots in these images, which represent the local variation in the nonlinear responses of individual meta-atoms, are likely to result from the local defects, such as random surface roughness and coupling of these metallic grain, that occasionally favor the generation of harmonic waves under specific excitation conditions.[46] Random features in nanoscale metallic structures, such as irregularly-shaped metal particles and fractured aggregates, are known to enable localized, enhanced nonlinear optical processes.[76] Despite the local hotspots in the SHG images resulting from the local defects of the sample, the micrometer-scale features of the GT logo, including the sharp corners and the boundary between the two enantiomer zones, are very well resolved within the excited region of the pattern. The contrast of the SHG images is an order of magnitude stronger than that of the linear images shown in Figure 2.12, thanks to the extraordinary large SHG-CD in our chiral metamaterial. To further illustrate the contrast produced by the enantiomers, a SHG-CD image (Figure 2.13b) was created by applying the formula mentioned above to the SHG images

in Figure 2.13a in a pixel-by-pixel manner. The equation that governs SHG-CD is extremely useful in differentiating between two chiral enantiomers in Figure 2.13b because it removes hot spots within our image. The defined contrast in this image provides an incredible ability in visualizing the chirality of metamaterial nanostructures.

2.7 Conclusions & Outlook

In this chapter, we built on the realm of chiroptics by using nonlinear imaging and spectroscopy to study the two artificial enantiomers of a twisted-arc metamaterial. As the significance of chiral plasmonic structures plays a larger role in the future of optoelectronic platforms, the greater the need will be for characterization, analysis, and maintenance techniques of these platforms. Nonlinear spectroscopy and imaging of chiral metamaterials offers a unique look into the functionality and deployability of these structures, and serves as a readily accessible and intensely accurate tool for the study of chirally sensitive materials. Chiral metamaterials offer a strong platform to induce SHG via their plasmonic resonances and by naturally interfering with the $\chi^{(2)}$ susceptibility tensor, making these artificial structures the perfect tool to initiate a study of chiral-selective nonlinear interactions. Future projects will seek to use chirality

and its more distinguishable nonlinear response to image not only metamaterials, but also chiral biological samples on metamaterials. In addition, these high-intensity probed chiral materials could also act as selective, nanoscale reactors by inducing position based, enantiomer selective reactions via resonance heating

CHAPTER III.

Metamaterials Enable Chiral-Selective Enhancement of Two-Photon Luminescence from Quantum Emitters

As natural chiral materials demonstrate limited circularly dichroic contrasts, enhancement of these polarization dependent signals has long been the focus of chiral metamaterial research. By manipulating the geometric chirality of resonant plasmonic nanostructures, we are capable of enhancing light confinement to amplify chiral modified, nonlinear signals from quantum emitters. The chiral center of the metamaterial is opened for direct access, where emitters occupy the most light-confining and chirally sensitive regions. The resulting two-photon emission profiles from circularly polarized excitations display mirrored symmetry for two enantiomer structures. The efficiency of the nonlinear signal directly correlates to the chiral resonance of the linear regime. The nonlinear emission signal is enhanced by 40× that of the emitters not embedded in the metamaterial and displays a 3× contrast for the opposite circular polarization. Such manipulations of nonlinear signals with metamaterials open pathways for

diverse applications where chiral selective signals are monitored, processed, and analyzed. In order to realize novel methods to enhance these linear chiroptical effects, traditional near-field studies, which probe the surface of a structure with an achiral emitter [77-79] have been attempted in the chiral linear regime to gain further insight.[80-82]

In this paper, we build on the realm of optical chirality that organic chemists have traversed by studying chiral metamaterials infused with achiral quantum emitters in order to probe the nonlinear, near-field interaction of engineered chiral structures. While the near-field of chiral, plasmonic structures has previously been numerically[23, 83, 84] and experimentally[85, 86] studied, the study of the nonlinear, near-field interactions remains sparse. In particular, very limited insights have been provided in the literature on how to access, probe and exploit the chiral selective hot spots generated in chiral engineered nanostructures. In this regard, further investigation is necessary as chiral metamaterials have demonstrated enhanced chiral responses orders of magnitude higher for their nonlinear counterparts due to symmetry breaking of the electrooptic tensor.[3, 46, 52] Specifically, this research focuses on selective enhancement of achiral quantum dot emitters within close proximity of our bi-layered, chiral metamaterial structure, which has tuned resonance and strong

circular dichroism. In particular, exposing the chiral center of the three-dimensional structure allows for probing and modification of the nonlinear signal at the heart of the metamaterial's structural chirality. Quantum dots (QD) are useful in studying this metal nanostructure because they offer tiny unit volumes for close structural proximity, large intensities, narrow band emission and a wide absorption range. However, placing semiconductor nanocrystals nearby metal structures breeds concern as quenching of the photonic energy by the metal structure is possible. For example, placing QDs in the vicinity of rough films enhances excitation, while placing them near smooth films causes quenching via Ohmic losses.[87-89] The enhancement recognized in the rough films can be attributed to the lightning rod effect, where rough surfaces lead to stronger confinement and larger mode volumes.[90] In order to achieve emission enhancement from this metallic yet luminescent complex, the current generated radiative enhancement outside the metallic structure must over power the non-radiative Ohmic losses inside the metallic structure.[89, 91] In general, the observed enhancement is associated with the existence of resonant features produced by the nearby chiral nanostructures.

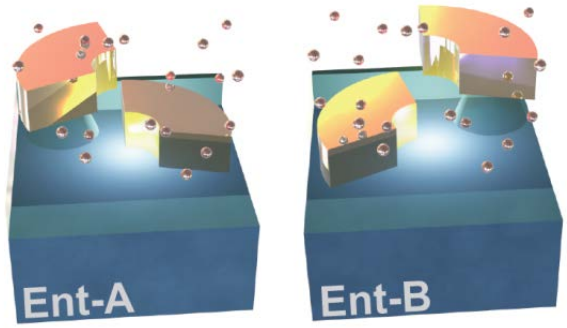

Figure 3.1: Schematic of enantiomer A (top) and enantiomer B (bottom) of the chiral metamaterial. QDs fill the volume mostly surrounding the region around the upper arc.

This project exhibits chiral manipulation of a locally emitted source and asymmetric enhancement of the nonlinear signal generated from two-photon excitation (TPE) of a nanocrystal emitter. The chiral contrast of the output nonlinear signal, two-photon luminescence (TPL), is witnessed when a circularly polarized input is incident on the near-field emitters embedded in the chiral arc structure. The subwavelength confinement and intense resonance provided by the silver arcs promotes selective enhancement and leads to pronounced nonlinear circular dichroism of the complex. The nonlinear signal offers a more distinguishable enhancement between circular polarizations than an input low intensity signal because TPE is a third-order nonlinear process, which enables the asymmetrically enhanced, chiral-selective behavior correlated to the meta-structure's spectral resonance in the linear regime. By employing geometrically

chiral structures to selectively enhance nonlinear optical effects a new brand of metamaterial is developed.

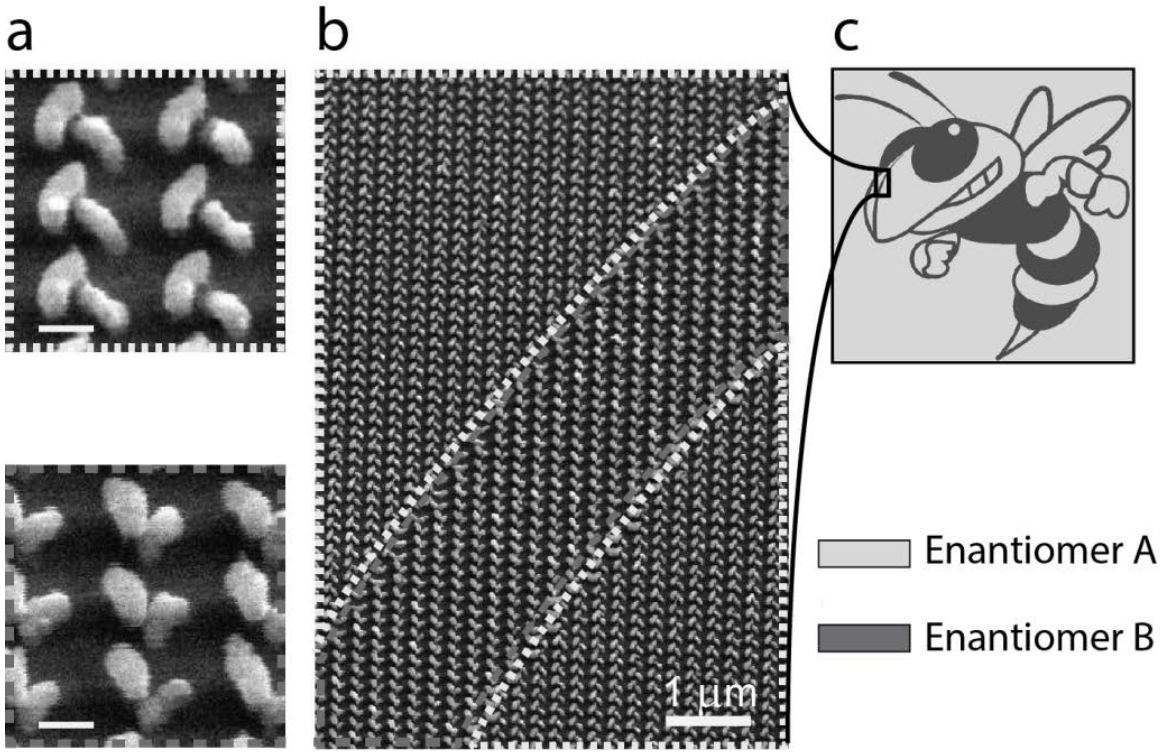

Figure 3.2: SEM images and nanoarc patterning **(a)** SEM images of the silver bi-layered structure of enantiomer A (top) and enantiomer B (bottom) before embedding the QDs. The scale bar in the figure represents 100 nm. Added roughness of the structure is due to plasma etching. (**b**) An SEM image of a patterned region involving both enantiomers. Here enantiomer B forms the inner portion of the line and enantiomer A the exterior portion. (**c**) A pattern of the GT mascot, 'Buzz,' that employs both enantiomers to provide the outline and color. Enantiomer A fills the light gray space outside and inside the pattern and Enantiomer B fills the darker regions.

3.1 Fabrication

The helicity of the chiral arc pair leverages the structural simplicity necessary to create augmented chiroptical properties. The silver, chiral metamaterial and its enantiomer pair are depicted in the schematic of Figure 3.1. The graphic illustrates that the QD-polymer coating occupies the entire space around the upper chiral arc and only a slight portion of the lower arc. Scanning electron microscopy images, seen in Figure 3.2a, illustrate the bi-layered structure prior to encapsulating the arcs in the QD-polymer solution. A slight, lateral shift of 30 nm affects the entire patterned region, but later shows little effect on the overall chiral properties of the material. The SEM image in Figure 3.2b captures a small segment of a pattern utilizing enantiomer A and B before QD embedment. The two enantiomers provide the internal coloring of the Georgia Tech, yellow jacket mascot pattern as seen in Figure 3.3c. The embedded CdSe/ZnS core-shell quantum dots have a range of absorption that extends from the ultraviolet up until their emission peak at 640 nm, which is identified by the dashed line in the first two plots of Figure 3.2. The emitting dots were chosen such that their emission peak corresponds with one of the two chiral resonances of the twisted arc metamaterial.

A 1 inch^2 piece of glass was coated with an 800 nm polymethyl methacrylate (PMMA) layer as an electron beam resist. The resist was spun at 1000 rpm for 60 seconds with 2 seconds of ramping time and baked for 90 seconds at 180 °C. A subsequent layer of water soluble conductive polymer, Espacer 300z, was spun on at 2000 rpm for 30 seconds and 1 second of ramping time. The layers were then patterned with alignment marks via an electron beam lithography system (JEOL JBX-9300FS EBL). The conductive layer is then removed with DI water. The resist was developed in a mixture of isopropyl alcohol, and methyl isobutyl ketone in a 1:1 volume ratio for 2 minutes. The alignment marks were then deposited. Electron beam deposition amassed a 10 nm later of titanium as an adhesion layer and a 200 nm layer of silver. Acetone solution lifted-off the residual PMMA structure to complete the patterning of the alignment marks. In order to pattern the bottom layer of the chiral arc metamaterial, a second run of electron beam lithography employing the alignment markers was accomplished by reiterating the above steps. Once lift-off was completed, spin on glass (IC1-200, Futurrex Inc.) was coated with a spin speed of 5000 rpm for 60 seconds with a 2 second ramping time. The solvents from the transparent dielectric were evaporated by heating the sample at 200 °C for 60 seconds. Plasma etching was performed to reduce the spacing between the

bottom of the upper arc and the substrate to 72 nm. From here another round of electron beam lithography was applied to define the second chiral arc.

After lift-off of the PMMA for the third time, the sample was then partially plasma etched furthering the surface area of the structure exposed to air. This etching removes another portion of the spin-on glass and is reduced by roughly 50 nm, thereby exposing part of the first chiral arc and leaving the upper chiral arc standing only via a pillar. A layer of polylauryl methacrylate (PLMA) doped with quantum dots was spin coated on the surface of this exposed chiral arc structure. The coating solution consisted of CdSe/ZnS core-shell quantum dots in a 1:6 ratio of QDs to 4% solution of PLMA in toluene. The volume concentration of QDs surrounding the metamaterial structure is approximately $1/40$ nm^3.

The completed chiral arc structure has the following parameters. The thickness of each arc is 42 nm and the width (from inner radius to outer radius) is 70 nm. The top of the lower arc is separated from the bottom of the upper chiral arc by roughly 30 nm. In enantiomer A, the upper arc is a quarter of a circle and has both of its horizontal faces aligned parallel to the walls of the unit cell. The lower arc is adjusted 15 degrees clockwise from the parallel face. The

periodicity of the unit cell is 225 nm. The enantiomer B is a mirror image of this structure.

3.2 Linear Response and Simulation

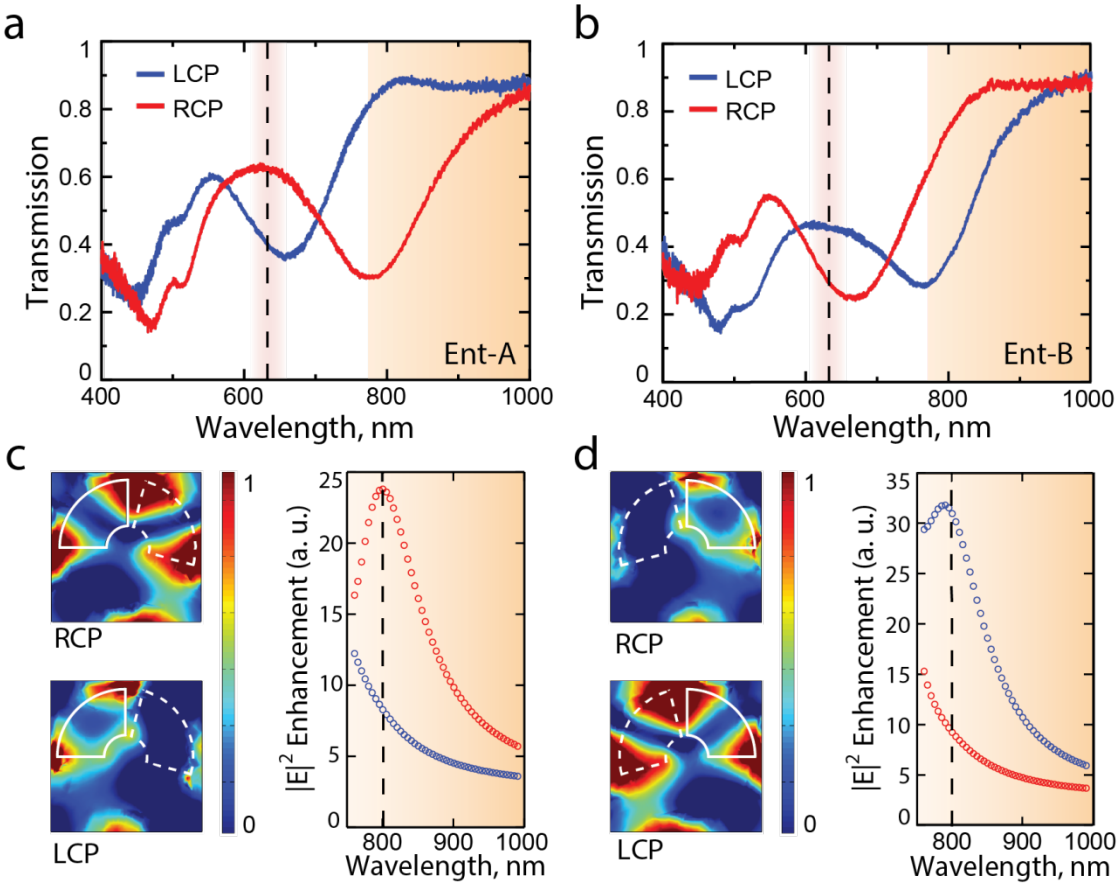

Figure 3.3: Chiral spectral resonances for selective enhancement. a) Transmission of LCP and RCP light incident on enantiomer A. An absorption resonance occurs at 640 nm for LCP incidence and another dip at 780 nm for RCP incidence. The dashed line accentuates the location of the QD emission wavelength and the grayed region displays the wavelengths that will be pumped to produce TPE. b) Similarly in enantiomer B, resonances occur at 640 and 780 nm; however, for opposite circular polarizations. c) $|E|^2$ field enhancement of enantiomer A under left and right circular polarizations. A cross sectional cut, half way between the upper and lower arc, visualizes the log-scaled and

normalized intensity of enantiomer A at 800 nm for RCP (top) and LCP (bottom). Simulation data for enantiomer A shows substantial enhancement of the intensity within the surrounding region of the chiral arc structure at a wavelength of 800 nm under RCP illumination. The simulation range (right) covers the pump wavelengths for the nonlinear excitation later performed. The dashed line corresponds to the spectral location where the $|E|^2$ maps are simulated. d) Chiral-selective field enhancement of enantiomer B. Cross sectional distributions of the $|E|^2$ are mirror images of the two enantiomers.

These chirally related, resonant dips in the arc's transmission profile, which can be seen in Figures 3.3a and 3.3b, occur at roughly 640 nm and 780 nm when probed with left and right circularly polarized beams respectively. The circular dichroism, which describes the transmission contrast between the two circular polarizations of opposite handedness, can reach as large as 50% at the wavelength of the chiral resonance. The transmission dips at these locations provide resonance based light confinement, which is mapped in Figures. 3.3c and 3.3d for both enantiomers respectively at λ=800 nm. This figure demonstrates the square of the magnitude of the electric field under both circular polarizations at a cross sectional cut, half way between the upper and lower arc. The cross sectional graphics provide a logarithmic scale in order to reduce the visual amplification of the intensity located at the edges of the chiral arcs, due to lightning rod effects. Higher squared, magnitudes of the electric field are observed for the circularly polarized illumination that corresponds to the transmission dip experienced for a specified enantiomer. For example, enantiomer A shows a

transmission dip at 800 nm for right circularly polarized light as seen in Figure 3.3a and thus a higher electric field magnitude squared as seen in Figure 3.3c (top). In comparison, the other circular polarization, Figure 3.3c (bottom) produces little intensity enhancement in the $|E|^2$ field map. Additional simulations were provided for the near-infrared regime, where the localized intensities were integrated within the surrounding region that the QDs were injected into. These simulations, plotted in the right of Figures 3.3c and 3.3d, demonstrate the strongest enhancement at a wavelength of 800 nm. A slight shift in the spectral, resonance location of enantiomer A in comparison to enantiomer B is shown and can be attributed to the asymmetry of the integration area, which corresponds to the location of the QDs hosted in the metamaterial structure. The spatially-averaged enhancement in $|E|^2$ reaches a factor of approximately 30 near the resonance peak, which in turn implies a substantial, chiral-selective enhancement in nonlinear light-matter interactions.

3.3 Optical characterization.

Linear transmission measurements of the metamaterial structure were performed by impinging circular polarized light onto the sample. A tungsten halogen light source was circularly polarized by employing a linear polarizer and a quarter

wave plate. An objective was used to magnify the transmitted signal and was selectively filtered to measure only the proper spectral regions. Linear imaging was achieved by switching the broadband light source with either a HeNe laser or a Ti-sapphire laser tuned to 800 nm.

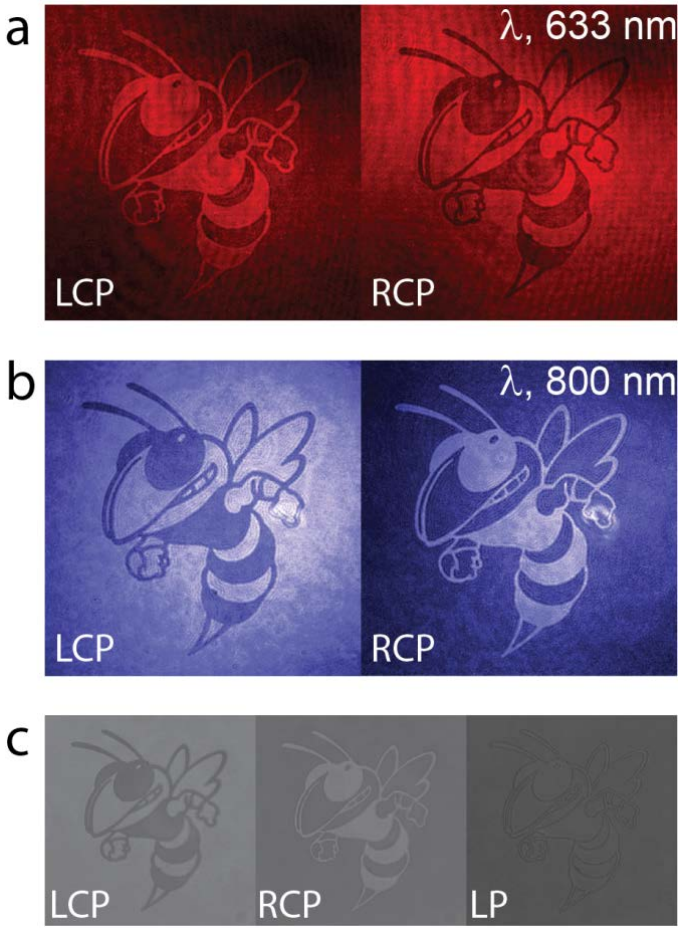

Figure 3.4: Linear transmission images of the GT mascot. a) Laser illuminated transmission image at 633nm for bother circular polarizations. The two colors in each picture are provided by the absorption or transmission of the light passing through one of the two enantiomers that compose the pattern b) Laser illumination with an 800nm source. c) Broadband illumination with a combination of filters around from 715-1000nm.

3.4 Imaging

Transmission images of the metamaterial pattern within their resonance bands of circular dichroism are provided in Figure 3.4. The same pattern of 'Buzz' the Georgia Tech mascot, which is composed of enantiomers A and B according to the pattern in Figure 3.2c, is imaged under different illumination conditions. These images are taken by impinging left or right circularly polarized light onto the patterned metamaterial region. As one of the circular polarization demonstrates low transmission for a specified enantiomer, the contrast produced between the two adjunct enantiomers at a specified resonant wavelength is very distinguishable. The first set of pictures is taken at the lower wavelength resonance of 633 nm and the second set, at the second resonance with λ=800 nm. Finally, three gray scaled graphics of 'Buzz' are shown in Figure 3.4c. The images are taken with a broadband source restricted to the near-infrared regime, 715 to 1000 nm, under three different polarizations, right circular, left circular and linear. The polarity of the images is related to the handedness of the circularly polarized illumination and a featureless gray image is produced under linearly polarized light. Having demonstrated the strength of our metamaterial to produce circularly polarized differentiation through these graphics, we will now

proceed to evaluate the chiral-selective nonlinear emission from this hybrid metamaterial system.

3.5 Two-photon luminescence

The goal of the QD embedded metamaterial is to characterize the near-field environment of the chiral arc structure with a fixed emission wavelength of 640 nm under varied excitation conditions. By illuminating the structure with a pulsed laser of high peak intensity, the nonlinear excitation of the QD-metamaterial complex leads to TPE of the QDs, which can be selectively enhanced depending on the incident circular polarization. The existence of TPE in semiconductor materials was first demonstrated in 1956,[92] but a recent usurping of the tool occurred when nanocrystalline, semiconducting structures became available. [83, 84, 93]

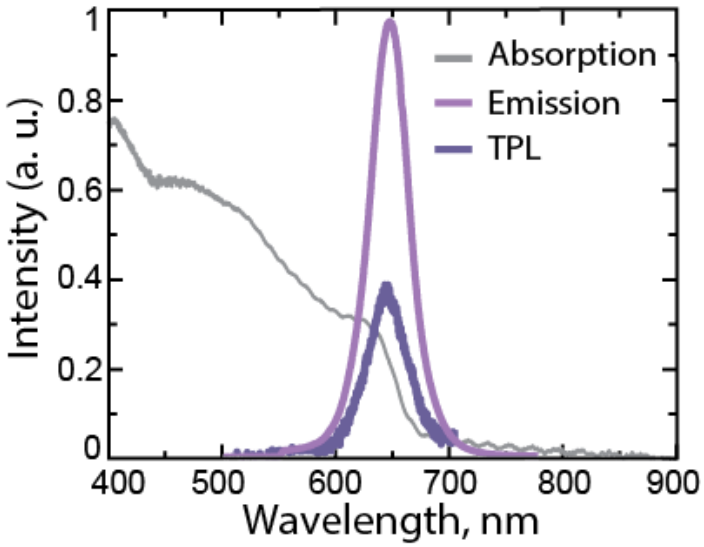

Figure 3.5: Emission profiles and absorption spectra for the embedded QDs. The absorption profile of the QDs demonstrates a characteristic cut off at a wavelength of 640 nm. The emission profile of the two-photon excitation is magnified in this image, as the two-photon excitation emission is orders of magnitude lower than the standard, emission profile under linear excitation.

In Figure 3.5 we show the typical absorption, linear emission and TPL profile of the QD-polymer coating. The two-photon excitation from the QD-polymer coating is scaled by many orders of magnitude in Figure 3.5a. The overlap of the linear and nonlinear emission peaks shows almost no spectral shift. The incident laser source at λ=800 nm was filtered to remove any unexpected light sources below 780 nm, thereby removing the possibility of lower wavelength excitation. The QD was also tested for circular polarization dependency by probing the substrate with left and right circular polarized beams. In this scenario, the QD emitted similar photon counts when probed with both polarizations, thereby removing any possibility of QD-circular polarization

dependency. In addition, since quantum dots blink and are known to charge over time,[88, 94] extended exposures and averaging of measurements were conducted.

3.6 Nonlinear Characterization

Two-photon excitation measurements were achieved by impinging circularly polarized light from a tunable pulsed laser onto the sample, using a similar circular polarizing setup. The pulse train has a repetition rate of 80 MHz and a pulse width of 100 fs. Control of the input power and polarization was achieved by two sets of Glan polarizers complimented with half wave plates. All nonlinear measurements except the intensity dependence of the metamaterial-QD complex were conducted at an input power of 2 mW and the QD substrate was measured at an input power of 10 mW. Power input measurements are explicitly stated in Figure 3.10. The spot size on the sample was roughly 60 μm^2. All measurements were conducted in ambient temperature.

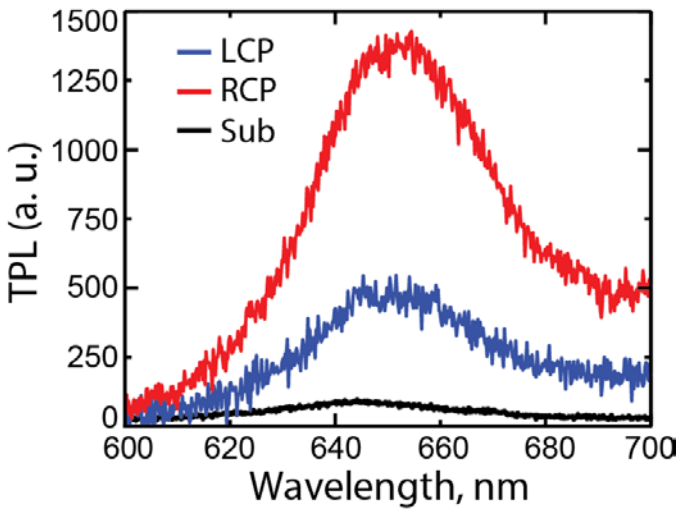

Figure 3.6: The two-photon excitation profile at 800 nm under different input circular polarizations for enantiomer A.

When embedded in the metamaterial, the QDs emit a higher TPL photon count than observed in just the polymer film of the same thickness and QD concentration, as seen in Figure 3.6. This figure displays the TPL enhancement from the metamaterial structure at a probe wavelength of 800 nm; this wavelength responds the most dramatically to the resonant conditions set by the chiral arc structure. The observed enhancement is attributed to the effectively increased absorption cross-sectional area of the QD. In addition, the emission enhancement from the QDs embedded in the metamaterial can be attributed to the resonant condition and confinement volume of the chiral arc pair, thereby intensifying the light energy in the nearby emitters. It should also be noted, that in Fig. 4b the two-photon luminescence peak of the QD on the substrate occurs at an expected wavelength of 640 nm, however the two-photon luminescence peak

of the QDs embedded in the metamaterial demonstrates a 10 nm red shift to 650 nm. This red shift is likely attributed to the spectrally dependent antenna effect from the metallic nanostructures. In addition, Figure 3.6 also shows an unusual asymmetry compared to the Gaussian shape of the QDs TPL. The increased emission profile seen at longer wavelengths, can be attributed to two-photon luminescence from the metal of the metamaterial structure.[95, 96] Special care was taken to eliminate any influences from the metal based two-photon luminescence in subsequent integration of these peaks.

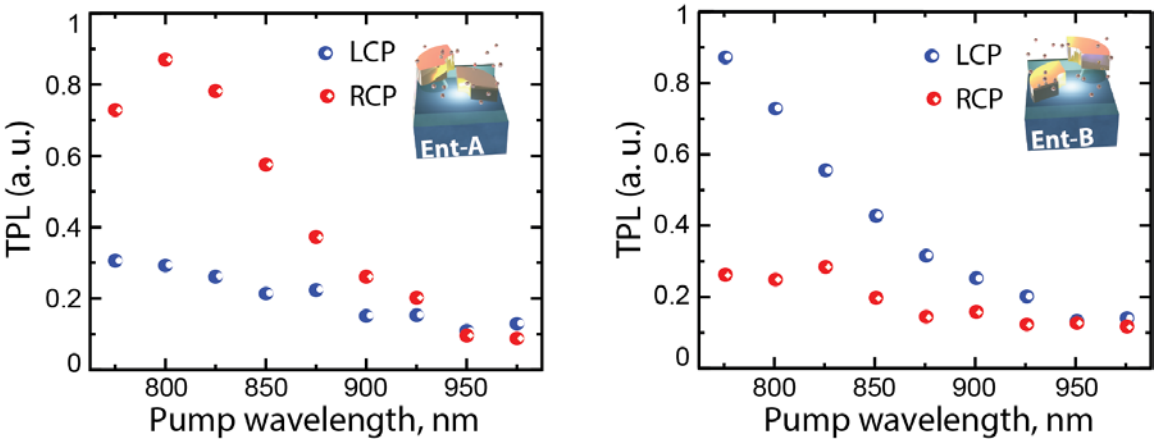

Figure 3.7: Two-photon excitation spectroscopy. The integrated two-photon emission profile for enantiomer A for both circular polarizations is shown on the left. Peaks similar to those seen in Figure 3.5 are integrated to resolve this figure. The two-photon excitation spectroscopy of enantiomer B again demonstrates reversed polarity for the two circular polarizations.

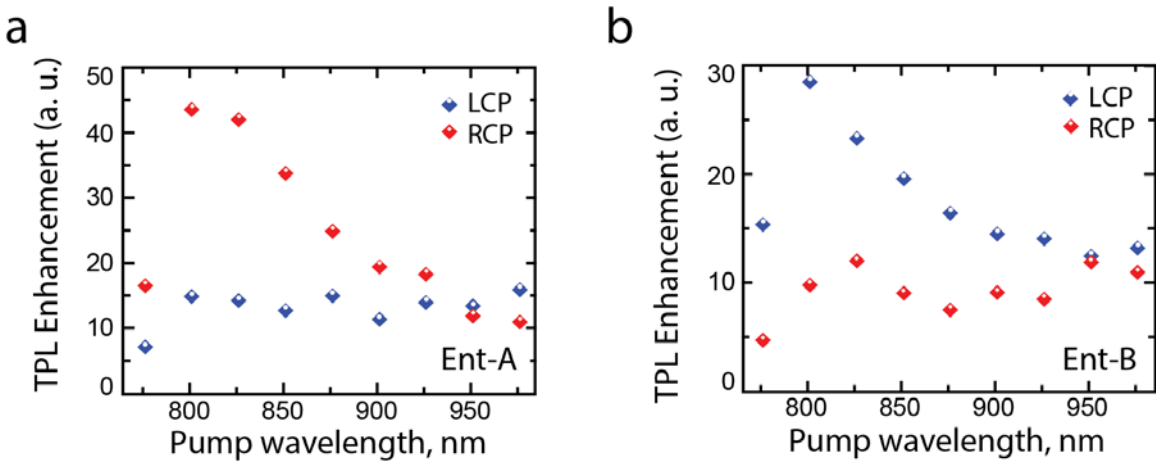

Figure 3.8: Chirally distinct two-photon luminescence. (a) Two-photon luminescence enhancement of enantiomer A under left and right circular polarizations. A large contrast between the two circular polarizations arises at 800 nm, where the linear excitation resonance occurs as seen in Figure 3.2c. The TPL enhancement is calculated by dividing the output luminescence from the QD-metamaterial complex by the luminescence from the QD film. (b) Enantiomer B shows switched magnitudes of TPL enhancement for the two circular polarizations.

In order to relate the near-field interactions of the metamaterial to its linear counterpart and gain a better understanding of the chiral, QD-nanoparticle interaction, a range of near-infrared wavelengths are probed under high peak power beams. Both enantiomers A and B are subjected to left and right circularly polarized light. The set of emission peaks obtained are similar to those shown in Figure 3.6. These peaks were integrated over a range of 80 nm to quantify the TPL intensity as a function of probe wavelength, from 775 to 975 nm, and the result is shown in Figures 3.7a and 3.7b. Enantiomer A demonstrates a significantly higher nonlinear signal for a RCP incident beam, as

predicted by the simulation in Figure 3.3c. This signal enhancement is mirrored by Enantiomer B for its respective resonant polarization in the near infrared regime, LCP light. The concept of a resonant polarization can only be discussed in a certain wavelength range, as outside of this limited range, the resonant polarization may switch. A couple distinct features are immediately noted in Figures 3.7a and 3.7b. For instance, the nonlinear contrast between the LCP and RCP beams drops substantially as the excitation wavelength moves away from the resonance peak around 800 nm. The bandwidth of this region is similar to the bandwidth of the linear circular dichroism region. As the nonlinear probed regime measurement is limited by the wavelength range of our system's setup, the overall circularly dichroic bandwidth of the nonlinear region might be larger. Moreover, these bandwidths occur at roughly the same spectral locations. For this reason, the reduced polarization dependency of the TPL at either end of the bandwidth can most likely be attributed to the resonance effects seen in the linear spectrum of Figure 3.3. Further extrapolating from Figure 3.3a and 3.3b, we note an increased absorption resonance for either right or left circular polarizations at wavelengths approaching 800 nm, for enantiomers A and B respectively. This linear resonance feature describes the relative emission maximum in Figure 3.7a, where the radiated nonlinear source is directly related,

to the light confining ability of the metamaterial. In this way, the maximum TPL peak takes on the spectral location of the linear absorption maximum (transmission minimum). This trend is followed throughout the entire probe spectrum, such that at spectral locations where there is minimal differentiation between the two circular polarizations in the linear regime, the nonlinear regime responds similarly.

The strong enhancement at the excitation wavelength of 800 nm introduces a disparate contrast in TPL between the two incident circular polarizations as seen in Figures 3.8a and 3.8b. Enantiomer A at this spectral location under RCP excitation demonstrates a chiral-TPL enhancement of 40× that of the QD substrate and an enhancement roughly 3× that for the LCP incident light. In mirror like contrast, the LCP excitation of enantiomer B demonstrates a distinction of 30× that of the QD-polymer coating and 3× that for the RCP excitation beam. The reduction of the enhancement for the non-resonant polarization demonstrates that the light confining ability of the structure is significantly reduced when the geometry of the mode is not aligned with that of the structure's chiral nature for a given wavelength. The enhancement of the resonant polarization for a given enantiomer is also significantly reduced as the probe wavelength deviates from the resonance peak

at 800 nm. The difference in the magnitude of enhancement from these two enantiomers is likely due to the asymmetric placement of the QDs in the metamaterial. Substantiating the enhancement data shown in Figures 3.8a and 3.8b, the series of simulations calculated for the same probe wavelengths that were supported by our high peak intensity laser source provides similar results, as seen in Figures 3.3c and 3.3d.

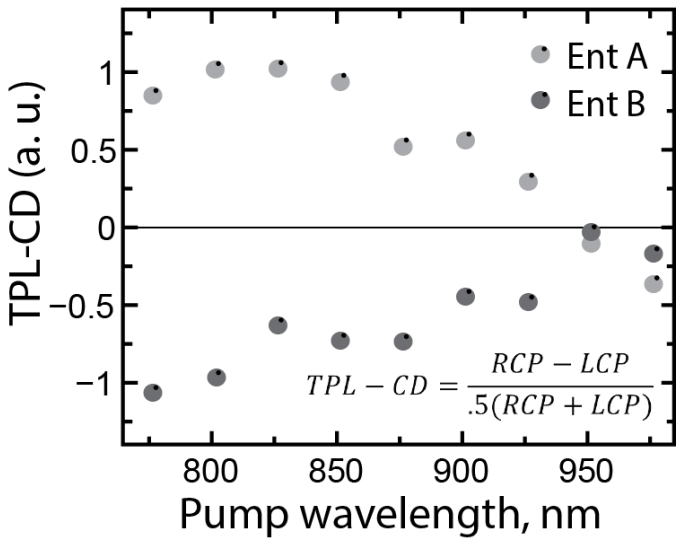

Figure 3.9: Two-photon luminescence - circular dichroism of QD's embedded in enantiomer A and B. TPL-CD is defined as the given equation in the figure and describes the difference in nonlinear output signal from the two circular polarizations. The circular dichroism is enhanced at the linear excitation resonance of the enantiomers.

The contrast of the nonlinear luminescence can be described by a figure of merit similar to linear circular dichroism. Two-photon luminescence-circular dichroism is defined as $TPL - CD = \frac{(RCP - LCP)}{.5(RCP + LCP)}$. This property provides a quick

understanding of the contrast that a chiral structure demonstrates based on the difference in two-photon emission from the two incident circular polarizations. Figure 3.9 demonstrates the contrast experienced from both circular polarizations on enantiomers A and B. The structures exhibit a flipped polarity in terms of TPL-CD which is demonstrated by the mirror symmetry presented across the x-axis of the plot. As chiral enhancement is increased at wavelengths approaching 800 nm, the two enantiomer structures show augmented TPL contrast.

Also shown in Figures 3.8a and 3.8b, the two-photon emission peak near 800 nm seems to be red-shifted from the linear spectrum's resonance dip at roughly 775 nm. However this red-shift may be anticipated as the spectral location of higher-order optical resonances often differs from that of their linear counterpart due to harmonic damping specifically in metals.[75] Based on this shift, it would seem that some damping occurs in the metamaterial as it is coupled into far-field transmission. In order to validate that the emission peak was in fact demonstrated from TPE and not by another linear source term, an analysis of power dependence was performed. Figure 3.10 demonstrates that TPE has a quadratic dependence on the input intensity for both the QDs in the metamaterial and on the substrate. The figure supplies a coefficient *K,* to describe the exponential dependence such that, $I_{2\omega} \propto I_{\omega}^{K}$, where $I_{2\omega}$ is the

intensity of the nonlinear signal and I_ω is the input probe beam intensity. The regression line of the logarithmic plot provides an exponential dependence of 2.0 $\pm$ 0.1 for the data points.

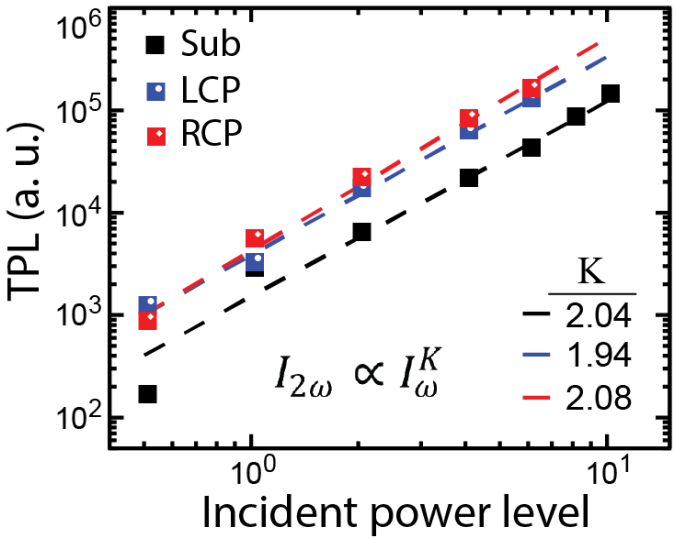

Figure 3.10: Two-photon luminescence as a function of the intensity of the pump light. All input polarizations demonstrate quasi-quadratic power dependence, evidencing two-photon excitation.

3.7 Conclusion

In this chapter, we demonstrate chiral-selective enhancement of two-photon luminescence from QDs embedded in a chiral metamaterial. The giant chiral response in a metamaterial, consisting of coupled nano-arcs, facilitates circular dichroic manipulation of the far-field intensity of locally emitted

nonlinear signals. In addition, the efficiency of the two-photon luminescence from the hybrid meta-system is directly correlated to the chiral resonance in the linear regime. By both, exposing the resonant near field of our chiral structure and inserting semiconductor nanocrystal emitters as indicators of localized chiral hotspots, we demonstrate two-photon enhancement of a chirally modified signal. Due to the light confining ability of the metamaterial under circularly polarized excitation, the two-photon luminescence from the hybrid system is enhanced by over 40 times with respect to a reference case without the metamaterial. The enhancement is chirality-enabled and is therefore sensitive to the handedness of the circularly polarized excitation; the enhancement factor demonstrates a contrast as large as 3 for the two circular polarizations observed in our experiment. Future works might look to reduce metallic particle quenching by introducing thin layered coatings around the metal structures and larger metallic spacing, thereby adding potential for nonlinear optical signal manipulation with reduced optical loss. This work represents a key demonstration in the realm of active chiral metamaterials, where the enhanced chiral fields are purposely exploited to enable chiral-selective light-matter interactions for imaging, sensing, and spectroscopic applications.

CHAPTER IV.

Conclusions and Outlook of Nonlinear Chiral Metamaterials

The need for large contrast from chiral responsive materials is necessary, whether it's for molecular sensing, realizing unique chiral enabled properties like negative refraction, or for imaging purposes. Nonlinear chiral responses offer the unique ability to take the existing contrast recognized in the linear domain and are able to enhance it significantly.

In both works presented here, the nonlinear responses showed enhanced circular dichroic contrast that spectroscopically mirrored the linear responses. The nonlinear responses incurred a slight broadening and spectral shift compared to that of the linear transmittance. This effect may be anticipated in the nonlinear responses as dampening of the incident light can occur, thereby shifting the frequency when the signal transitions to its higher order signals.

Chapter two sought to increase the circular dichroic contrast between the two circular polarizations incident on the metamaterial structure. A brief overview of what was achieved in chapter 2 is presented in Figure 4.1. The second harmonic signal produced immense contrast between the two circular

polarizations at the metamaterials resonant wavelength of 800 nm. This enormous contrast, roughly 20x, can be seen in the imaging demonstration, where the light emitted from one enantiomer under RCP illumination is proportionally zero compared to the brightness of the other enantiomer. As we move away from the resonant wavelength the contrast fades off.

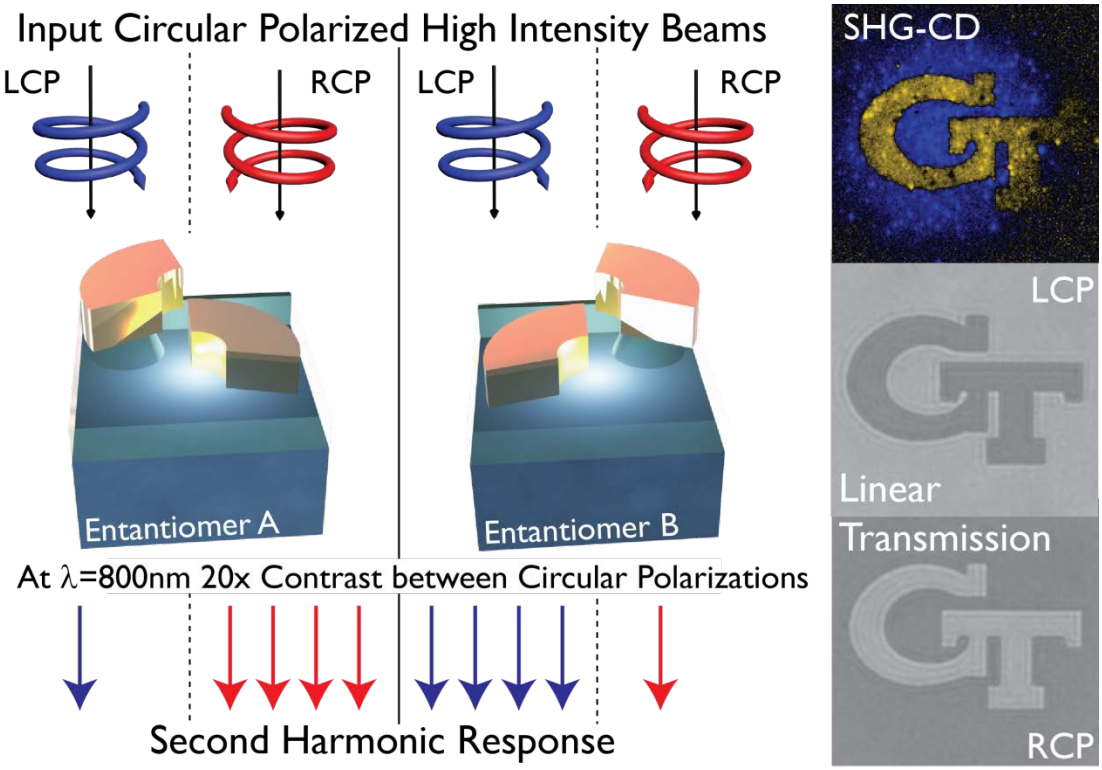

Figure 4.1: Overview of how to produce enhanced contrast from nonlinear responses of chiral nanoarc metamaterials. When right circularly polarized (RCP) light is incident on the metamaterial a second harmonic response is generated that is 20x that of the LCP light. Complementarily, enantiomer B produces the higher response for the opposite circular polarization. Two enantiomers make up an array of a metamaterial structure, where the GT is filled with enantiomer B and the exterior enantiomer A. SHG-CD is the normalized circular dichroic

contrast generated by the second harmonic signal.

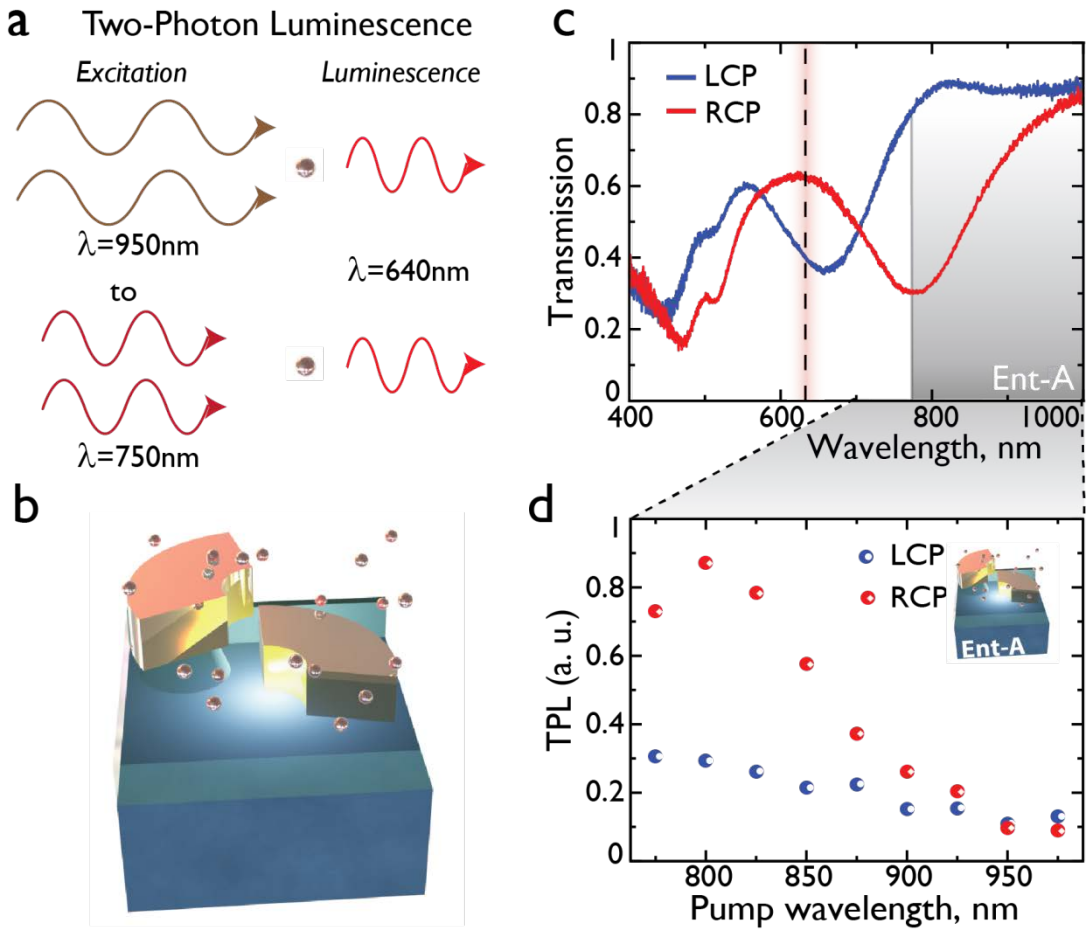

Figure 4.2: Scheme for extracting circular dichroic response via a luminescent signal. (a) Two photon luminescence. Wavelengths distributed between 750 and 950 nm are incident on a set of quantum dots. The high intensity beam causes the QD's to absorb two photons at this long wavelength and luminesce at its emission wavelength of 640 nm. (b) The QDs are injected into the chiral hot spots of the chiral nanoarcs. (c) The chiral metamaterial has a large circular dichroic response at 640 nm, where CD is the difference between transmission of left and right circularly polarized beams. (d) The enhanced signal contrast generated from the quantum dots embedded in the chiral metamaterial structure.

Chapter 3 sought to access the chiral hotspots of our twisted arc metamaterial to produce enhanced, nonlinear responses from an achiral emitter.

A brief overview of what was achieved in Chapter 3 is presented in Figure 4.2. The contrast between circular polarizations is roughly 4x. Moreover, the chiral arcs enhanced the two-photon luminescent signal up to 44x at the resonant wavelength of the chiral arcs, thus providing ample contrast from background emission. Chiral metamaterials have their widest applications in sensing. With the help of this work, we hope to push forward this realization of using chiral metamaterials for sensing purposes. However, this work may open doors for optical signaling or detection devices for communications, characterization techniques, and optical components as well.

Outlook : Extracting Chiral Signals

The future of this research will look to utilize secondary methods to measure chirality through well-established topics such as Rayleigh optical activity, which utilizes the scattered light to measure chirality. With this technique susceptibility tensor components can be measured. Other techniques that might be useful in extracting chiral information include circularly polarized luminescence (CPL) and fluorescence detected spectroscopy (FDCD). While CPL describes chirality as experienced in the excited state, FDCD describes chirality as experienced in the ground state.[97] These techniques provide similar information to circular dichroism and optical rotation but provide a different

method to extract the information which could be crucial to unlocking future uses of hybrid metamaterials.

Active & Switchable Metamaterials

Chirality by nature is Boolean and causes an instinctive desire to try and create a single metamaterial structure that could provide bother enantiomeric responses. In this case, using only a single circular polarization as incidence, but creating a different response based on the material properties. However, optical activity tends to stem from the configurational structure of that material. For this reason, in order to generate an optically active signal from a structure, the structure should be engineered such that it has a mirror image that cannot be superposed onto itself. To this end, the structure must be reconfigurable or utilize a property that would disengage the resonance of the structure. Switchable chiral metamaterials were briefly mentioned in the introduction.

Nonlinear Optical Activity

In a similar vein to switchable chirality, nonlinear optical activity is a process by which nonlinear dampening in the sample either through thermal or electrical sources, causes the chiral distinction provided by the material to fade. [98-100] To achieve this degradation of the chiral response, a high intensity beam is incident on the sample. The appearance of this effect was first observed in 1926[101], in a piece of uranium doped glass, which then lead to a series of very meticulous research papers.[102-104] The most recent contribution to the field was released within the past 4 years. The most recent task utilized a 2D

metamaterial at angled incidence to generate decreased absorption at higher pump intensities, utilizing a single shot experiment as to not mix their thermal and electrical responses.[105]

The outlook for nonlinear chiral metamaterials is bright. The work presented here having shown such immense enhancement in chiral contrast of the optical signals emitted from within the metamaterial provides us with a strong promise for future applications and unique nonlinear phenomena that can be presented through nonlinear interactions of these structures. As chiral metamaterials become more easily scalable, gain higher quality of design to sculpt the 3D helical light fields, chiral metamaterials will continue to demonstrate stronger chiroptical effects leading to more applications and potential for redefining the use of chirality in inorganic media.

REFERENCES

[1] W. Cai and V. Shalaev, *Optical Metamaterials Fundamentals and Applications*. New York, NY: Springer Science+Business Media LLC, 2010.

[2] N. I. Zheludev, "The Road Ahead for Metamaterials," *Science,* vol. 328, pp. 582-583, Apr 30 2010.

[3] S. P. Rodrigues, S. F. Lan, L. Kang, Y. H. Cui, and W. S. Cai, "Nonlinear Imaging and Spectroscopy of Chiral Metamaterials," *Advanced Materials,* vol. 26, pp. 6157-+, Sep 17 2014.

[4] S. P. Rodrigues, Y. H. Cui, S. F. Lan, L. Kang, and W. S. Cai, "Metamaterials Enable Chiral-Selective Enhancement of Two-Photon Luminescence from Quantum Emitters," *Advanced Materials,* vol. 27, pp. 1124-1130, Feb 11 2015.

[5] L. Barron, *Molecular Light Scattering and Optical Activity*, 2nd ed.: Cambridge, 2004.

[6] K. P. C. Vollhardt and N. E. Schore, *Organic Chemistry : Structure and Function*, 7. ed. New York, N.Y.: W.H. Freeman & Company, 2014.

[7] N. Berova, K. o. Nakanishi, and R. Woody, *Circular Dichroism: Principles and Applications*, 2nd ed. New York: Wiley-VCH, 2000.

[8] E. Hendry, T. Carpy, J. Johnston, M. Popland, R. V. Mikhaylovskiy, A. J. Lapthorn*, et al.*, "Ultrasensitive detection and characterization of biomolecules using superchiral fields," *Nature Nanotechnology,* vol. 5, pp. 783-787, Nov 2010.

[9] S. Sioncke, T. Verbiest, and A. Persoons, "Second-order nonlinear optical properties of chiral materials," *Materials Science & Engineering R-Reports,* vol. 42, pp. 115-155, Nov 15 2003.

[10] P. J. Ramberg, *Chemical Structure, Spatial Arrangement: The Early History of Stereochemistry, 1874-1914*: Ashgate Publishing, Limited, 2003.

[11] H. H. Thoen, M. J. How, T. H. Chiou, and J. Marshall, "A Different Form of Color Vision in Mantis Shrimp," *Science,* vol. 343, pp. 411-413, Jan 24 2014.

[12] D. H. Goldstein, "Polarization properties of Scarabaeidae," *Applied Optics,* vol. 45, pp. 7944-7950, Oct 20 2006.

[13] E. Libby, D. E. Azofeifa, M. Hernandez-Jimenez, C. Barboza-Aguilar, A. Solis, I. Garcia-Aguilar*, et al.*, "Light reflection by the cuticle of C. aurigans scarabs: a biological broadband reflector of left handed circularly polarized light," *Journal of Optics,* vol. 16, Aug 2014.

[14] V. Sharma, M. Crne, J. O. Park, and M. Srinivasarao, "Structural Origin of Circularly Polarized Iridescence in Jeweled Beetles," *Science,* vol. 325, pp. 449-451, Jul 24 2009.

[15] H. Lee, M. J. Huttunen, K. J. Hsu, M. Partanen, G. Y. Zhuo, M. Kauranen*, et al.*, "Chiral imaging of collagen by second-harmonic generation circular dichroism," *Biomedical Optics Express,* vol. 4, pp. 909-916, Jun 1 2013.

[16] T. Verbiest, M. Kauranen, A. Persoons, M. Ikonen, J. Kurkela, and H. Lemmetyinen, "Nonlinear-Optical Activity and Biomolecular Chirality," *Journal of the American Chemical Society,* vol. 116, pp. 9203-9205, Oct 5 1994.

[17] P. J. Campagnola, M. D. Wei, A. Lewis, and L. M. Loew, "High-resolution nonlinear optical imaging of live cells by second harmonic generation," *Biophysical Journal,* vol. 77, pp. 3341-3349, Dec 1999.

[18] M. A. Belkin and Y. R. Shen, "Non-linear optical spectroscopy as a novel probe for molecular chirality," *International Reviews in Physical Chemistry,* vol. 24, pp. 257-299, Apr 2005.

[19] T. Petrallimallow, T. M. Wong, J. D. Byers, H. I. Yee, and J. M. Hicks, "Circular-Dichroism Spectroscopy at Interfaces - a Surface 2nd Harmonic-Generation Study," *Journal of Physical Chemistry,* vol. 97, pp. 1383-1388, Feb 18 1993.

[20] J. D. Byers, H. I. Yee, T. Petrallimallow, and J. M. Hicks, "2nd-Harmonic Generation Circular-Dichroism Spectroscopy from Chiral Monolayers," *Physical Review B,* vol. 49, pp. 14643-14647, May 15 1994.

[21] P. Fischer and F. Hache, "Nonlinear optical spectroscopy of chiral molecules," *Chirality,* vol. 17, pp. 421-437, Oct 2005.

[22] E. Plum, V. A. Fedotov, A. S. Schwanecke, N. I. Zheludev, and Y. Chen, "Giant optical gyrotropy due to electromagnetic coupling," *Applied Physics Letters,* vol. 90, May 28 2007.

[23] X. H. Yin, M. Schaferling, B. Metzger, and H. Giessen, "Interpreting Chiral Nanophotonic Spectra: The Plasmonic Born-Kuhn Model," *Nano Letters,* vol. 13, pp. 6238-6243, Dec 2013.

[24] M. Hentschel, M. Schaferling, T. Weiss, N. Liu, and H. Giessen, "Three-Dimensional Chiral Plasmonic Oligomers," *Nano Letters,* vol. 12, pp. 2542-2547, May 2012.

[25] C. Helgert, E. Pshenay-Severin, M. Falkner, C. Menzel, C. Rockstuhl, E. B. Kley*, et al.*, "Chiral Metamaterial Composed of Three-Dimensional Plasmonic Nanostructures," *Nano Letters,* vol. 11, pp. 4400-4404, Oct 2011.

[26] M. Decker, S. Linden, and M. Wegener, "Coupling effects in low-symmetry planar split-ring resonator arrays," *Optics Letters,* vol. 34, pp. 1579-1581, May 15 2009.

[27] Y. Zhao, M. A. Belkin, and A. Alu, "Twisted optical metamaterials for planarized ultrathin broadband circular polarizers," *Nature Communications,* vol. 3, May 2012.

[28] V. K. Valev, J. J. Baumberg, C. Sibilia, and T. Verbiest, "Chirality and Chiroptical Effects in Plasmonic Nanostructures: Fundamentals, Recent Progress, and Outlook," *Advanced Materials,* vol. 25, pp. 2517-2534, May 14 2013.

[29] C. M. Soukoulis and M. Wegener, "Past achievements and future challenges in the development of three-dimensional photonic metamaterials," *Nature Photonics,* vol. 5, pp. 523-530, Sep 2011.

[30] Z. Li, M. Gokkavas, and E. Ozbay, "Manipulation of Asymmetric Transmission in Planar Chiral Nanostructures by Anisotropic Loss (vol 7, pg 482, 2013)," *Advanced Optical Materials,* vol. 1, pp. 608-608, Sep 2013.

[31] W. S. Gao, H. M. Leung, Y. H. Li, H. Chen, and W. Y. Tam, "Circular dichroism in double-layer metallic crossed-gratings (vol 13, 115101, 2011)," *Journal of Optics,* vol. 13, Dec 2011.

[32] J. C. Bose, "On the rotation of plane of polarisation of electric waves by a Twisted Structure," *Proceedings of the Royal Society of London,* vol. 63, February 14 1898.

[33] J. B. Pendry, "A chiral route to negative refraction," *Science,* vol. 306, pp. 1353-1355, Nov 19 2004.

[34] S. Zhang, Y. S. Park, J. S. Li, X. C. Lu, W. L. Zhang, and X. Zhang, "Negative Refractive Index in Chiral Metamaterials," *Physical Review Letters,* vol. 102, Jan 16 2009.

[35] J. K. Gansel, M. Thiel, M. S. Rill, M. Decker, K. Bade, V. Saile*, et al.*, "Gold Helix Photonic Metamaterial as Broadband Circular Polarizer," *Science,* vol. 325, pp. 1513-1515, Sep 18 2009.

[36] M. D. Turner, M. Saba, Q. M. Zhang, B. P. Cumming, G. E. Schroder-Turk, and M. Gu, "Miniature chiral beamsplitter based on gyroid photonic crystals," *Nature Photonics,* vol. 7, pp. 801-805, Oct 2013.

[37] B. N. Wang, J. F. Zhou, T. Koschny, M. Kafesaki, and C. M. Soukoulis, "Chiral metamaterials: simulations and experiments," *Journal of Optics a-Pure and Applied Optics,* vol. 11, Nov 2009.

[38] S. Zhang, J. F. Zhou, Y. S. Park, J. Rho, R. Singh, S. Nam*, et al.*, "Photoinduced handedness switching in terahertz chiral metamolecules," *Nature Communications,* vol. 3, Jul 2012.

[39] Y. Z. He, G. K. Larsen, W. Ingram, and Y. P. Zhao, "Tunable Three-Dimensional Helically Stacked Plasmonic Layers on Nanosphere Monolayers," *Nano Letters,* vol. 14, pp. 1976-1981, Apr 2014.

[40] M. Decker, R. Zhao, C. M. Soukoulis, S. Linden, and M. Wegener, "Twisted split-ring-resonator photonic metamaterial with huge optical activity," *Optics Letters,* vol. 35, pp. 1593-1595, May 15 2010.

[41] M. Decker, M. Ruther, C. E. Kriegler, J. Zhou, C. M. Soukoulis, S. Linden*, et al.*, "Strong optical activity from twisted-cross photonic metamaterials," *Optics Letters,* vol. 34, pp. 2501-2503, Aug 15 2009.

[42] S. Vignolini, N. A. Yufa, P. S. Cunha, S. Guldin, I. Rushkin, M. Stefik*, et al.*, "A 3D Optical Metamaterial Made by Self-Assembly," *Advanced Materials,* vol. 24, pp. Op23-Op27, Mar 8 2012.

[43] E. Plum, V. A. Fedotov, and N. I. Zheludev, "Optical activity in extrinsically chiral metamaterial," *Applied Physics Letters,* vol. 93, Nov 10 2008.

[44] V. A. Fedotov, P. L. Mladyonov, S. L. Prosvirnin, A. V. Rogacheva, Y. Chen, and N. I. Zheludev, "Asymmetric propagation of electromagnetic waves through a planar chiral structure," *Physical Review Letters,* vol. 97, Oct 20 2006.

[45] S. V. Zhukovsky, C. Kremers, and D. N. Chigrin, "Plasmonic rod dimers as elementary planar chiral meta-atoms," *Optics Letters,* vol. 36, pp. 2278-2280, Jun 15 2011.

[46] M. J. Huttunen, G. Bautista, M. Decker, S. Linden, M. Wegener, and M. Kauranen, "Nonlinear chiral imaging of subwavelength-sized twisted-cross gold nanodimers [Invited]," *Optical Materials Express,* vol. 1, pp. 46-56, May 1 2011.

[47] Y. H. Cui, L. Kang, S. F. Lan, S. Rodrigues, and W. S. Cai, "Giant Chiral Optical Response from a Twisted-Arc Metamaterial," *Nano Letters,* vol. 14, pp. 1021-1025, Feb 2014.

[48] A. V. Rogacheva, V. A. Fedotov, A. S. Schwanecke, and N. I. Zheludev, "Giant gyrotropy due to electromagnetic-field coupling in a bilayered chiral structure," *Physical Review Letters,* vol. 97, Oct 27 2006.

[49] R. A. Shelby, D. R. Smith, and S. Schultz, "Experimental verification of a negative index of refraction," *Science,* vol. 292, pp. 77-79, Apr 6 2001.

[50] M. Decker, M. W. Klein, M. Wegener, and S. Linden, "Circular dichroism of planar chiral magnetic metamaterials," *Optics Letters,* vol. 32, pp. 856-858, Apr 1 2007.

[51] J. F. Zhou, J. F. Dong, B. N. Wang, T. Koschny, M. Kafesaki, and C. M. Soukoulis, "Negative refractive index due to chirality," *Physical Review B,* vol. 79, Mar 2009.

[52] V. K. Valev, X. Zheng, C. G. Biris, A. V. Silhanek, V. Volskiy, B. De Clercq*, et al.*, "The origin of second harmonic generation hotspots in chiral optical metamaterials [Invited]," *Optical Materials Express,* vol. 1, pp. 36-45, May 1 2011.

[53] M. Schaferling, X. H. Yin, and H. Giessen, "Formation of chiral fields in a symmetric environment," *Optics Express,* vol. 20, pp. 26326-26336, Nov 19 2012.

[54] V. K. Valev, N. Smisdom, A. V. Silhanek, B. De Clercq, W. Gillijns, M. Ameloot*, et al.*, "Plasmonic Ratchet Wheels: Switching Circular Dichroism by Arranging Chiral Nanostructures," *Nano Letters,* vol. 9, pp. 3945-3948, Nov 2009.

[55] J. F. Dong, J. F. Zhou, T. Koschny, and C. Soukoulis, "Bi-layer cross chiral structure with strong optical activity and negative refractive index," *Optics Express,* vol. 17, pp. 14172-14179, Aug 3 2009.

[56] G. K. Larsen, Y. Z. He, J. Wang, and Y. P. Zhao, "Scalable Fabrication of Composite Ti/Ag Plasmonic Helices: Controlling Morphology and Optical Activity by Tailoring Material Properties," *Advanced Optical Materials,* vol. 2, pp. 245-249, Mar 2014.

[57] R. Schreiber, N. Luong, Z. Y. Fan, A. Kuzyk, P. C. Nickels, T. Zhang*, et al.*, "Chiral plasmonic DNA nanostructures with switchable circular dichroism," *Nature Communications,* vol. 4, Dec 2013.

[58] R. W. Boyd, "Nonlinear Optics, 3rd Edition," *Nonlinear Optics, 3rd Edition,* pp. 1-613, 2008.

[59] B. E. A. Saleh and M. C. Teich, *Fundamentals of photonics*, 2nd ed. Hoboken, N.J.: Wiley, 2007.

[60] W. S. Cai, A. P. Vasudev, and M. L. Brongersma, "Electrically Controlled Nonlinear Generation of Light with Plasmonics," *Science,* vol. 333, pp. 1720-1723, Sep 23 2011.

[61] V. K. Valev, A. V. Silhanek, N. Smisdom, B. De Clercq, W. Gillijns, O. A. Aktsipetrov*, et al.*, "Linearly polarized second harmonic generation microscopy reveals chirality (vol 18, pg 8286, 2010)," *Optics Express,* vol. 19, pp. 9242-9244, May 9 2011.

[62] E. A. Mamonov, T. V. Murzina, I. A. Kolmychek, A. I. Maydykovsky, V. K. Valev, A. V. Silhanek*, et al.*, "Chirality in nonlinear-optical response of planar G-shaped nanostructures," *Optics Express,* vol. 20, pp. 8518-8523, Apr 9 2012.

[63] M. Kauranen and A. V. Zayats, "Nonlinear plasmonics," *Nature Photonics,* vol. 6, pp. 737-748, Nov 2012.

[64] G. A. Wurtz, R. Pollard, W. Hendren, G. P. Wiederrecht, D. J. Gosztola, V. A. Podolskiy*, et al.*, "Designed ultrafast optical nonlinearity in a plasmonic nanorod metamaterial enhanced by nonlocality," *Nature Nanotechnology,* vol. 6, pp. 106-110, Feb 2011.

[65] M. W. Klein, C. Enkrich, M. Wegener, and S. Linden, "Second-harmonic generation from magnetic metamaterials," *Science,* vol. 313, pp. 502-504, Jul 28 2006.

[66] S. Linden, F. B. P. Niesler, J. Forstner, Y. Grynko, T. Meier, and M. Wegener, "Collective Effects in Second-Harmonic Generation from Split-Ring-Resonator Arrays," *Physical Review Letters,* vol. 109, Jul 6 2012.

[67] M. H. Li, L. Y. Guo, J. F. Dong, and H. L. Yang, "An ultra-thin chiral metamaterial absorber with high selectivity for LCP and RCP waves," *Journal of Physics D-Applied Physics,* vol. 47, May 9 2014.

[68] E. Plum and N. I. Zheludev, "Chiral mirrors," *Applied Physics Letters,* vol. 106, Jun 1 2015.

[69] N. Y. Ha, Y. Ohtsuka, S. M. Jeong, S. Nishimura, G. Suzaki, Y. Takanishi*, et al.*, "Fabrication of a simultaneous red-green-blue reflector using single-pitched cholesteric liquid crystals," *Nature Materials,* vol. 7, pp. 43-47, Jan 2008.

[70] Y. Q. Tang and A. E. Cohen, "Enhanced Enantioselectivity in Excitation of Chiral Molecules by Superchiral Light," *Science,* vol. 332, pp. 333-336, Apr 15 2011.

[71] F. Neubrech, A. Pucci, T. W. Cornelius, S. Karim, A. Garcia-Etxarri, and J. Aizpurua, "Resonant Plasmonic and Vibrational Coupling in a Tailored Nanoantenna for Infrared Detection," *Physical Review Letters,* vol. 101, Oct 10 2008.

[72] I. Ament, J. Prasad, A. Henkel, S. Schmachtel, and C. Sonnichsen, "Single Unlabeled Protein Detection on Individual Plasmonic Nanoparticles," *Nano Letters,* vol. 12, pp. 1092-1095, Feb 2012.

[73] V. G. Kravets, F. Schedin, R. Jalil, L. Britnell, R. V. Gorbachev, D. Ansell*, et al.*, "Singular phase nano-optics in plasmonic metamaterials for label-free single-molecule detection," *Nature Materials,* vol. 12, pp. 304-309, Apr 2013.

[74] X. L. Ma, C. Huang, M. B. Pu, C. G. Hu, Q. Feng, and X. G. Luo, "Multi-band circular polarizer using planar spiral metamaterial structure," *Optics Express,* vol. 20, pp. 16050-16058, Jul 2 2012.

[75] J. Zuloaga and P. Nordlander, "On the Energy Shift between Near-Field and Far-Field Peak Intensities in Localized Plasmon Systems," *Nano Letters,* vol. 11, pp. 1280-1283, Mar 2011.

[76] A. K. Sarychev and V. M. Shalaev, "Electromagnetic field fluctuations and optical nonlinearities in metal-dielectric composites," *Physics Reports-Review Section of Physics Letters,* vol. 335, pp. 276-371, Sep 2000.

[77] X. S. Xie and R. C. Dunn, "Probing Single-Molecule Dynamics," *Science,* vol. 265, pp. 361-364, Jul 15 1994.

[78] R. R. Chance, A. Prock, and R. Silbey, "Molecular Fluorescence and Energy Transfer Near Interfaces," in *Advances in Chemical Physics*. vol. 37, ed: John Wiley & Sons, Inc., 2007, pp. 1-65.

[79] C. Hoppener, Z. J. Lapin, P. Bharadwaj, and L. Novotny, "Self-Similar Gold-Nanoparticle Antennas for a Cascaded Enhancement of the Optical Field," *Physical Review Letters,* vol. 109, Jul 6 2012.

[80] A. O. Govorov, Z. Y. Fan, P. Hernandez, J. M. Slocik, and R. R. Naik, "Theory of Circular Dichroism of Nanomaterials Comprising Chiral Molecules and Nanocrystals: Plasmon Enhancement, Dipole Interactions, and Dielectric Effects," *Nano Letters,* vol. 10, pp. 1374-1382, Apr 2010.

[81] T. Nakashima, Y. Kobayashi, and T. Kawai, "Optical Activity and Chiral Memory of Thiol-Capped CdTe Nanocrystals," *Journal of the American Chemical Society,* vol. 131, pp. 10342-1343, Aug 5 2009.

[82] S. D. Elliott, M. P. Moloney, and Y. K. Gun'ko, "Chiral shells and achiral cores in CdS quantum dots," *Nano Letters,* vol. 8, pp. 2452-2457, Aug 2008.

[83] S. C. Pu, M. J. Yang, C. C. Hsu, C. W. Lai, C. C. Hsieh, S. H. Lin*, et al.*, "The empirical correlation between size and two-photon absorption cross section of CdSe and CdTe quantum dots," *Small,* vol. 2, pp. 1308-1313, Nov 2006.

[84] G. S. He, K. T. Yong, Q. D. Zheng, Y. Sahoo, A. Baev, A. I. Ryasnyanskiy*, et al.*, "Multi-photon excitation properties of CdSe quantum dots solutions and optical limiting behavior in infrared range," *Optics Express,* vol. 15, pp. 12818-12833, Oct 1 2007.

[85] Y. Q. Tang, L. Sun, and A. E. Cohen, "Chiroptical hot spots in twisted nanowire plasmonic oscillators," *Applied Physics Letters,* vol. 102, Jan 28 2013.

[86] N. Meinzer, E. Hendry, and W. L. Barnes, "Probing the chiral nature of electromagnetic fields surrounding plasmonic nanostructures," *Physical Review B,* vol. 88, Jul 29 2013.

[87] D. E. Chang, A. S. Sorensen, P. R. Hemmer, and M. D. Lukin, "Strong coupling of single emitters to surface plasmons," *Physical Review B,* vol. 76, Jul 2007.

[88] K. T. Shimizu, W. K. Woo, B. R. Fisher, H. J. Eisler, and M. G. Bawendi, "Surface-enhanced emission from single semiconductor nanocrystals," *Physical Review Letters,* vol. 89, Sep 9 2002.

[89] S. Kuhn, U. Hakanson, L. Rogobete, and V. Sandoghdar, "Enhancement of single-molecule fluorescence using a gold nanoparticle as an optical nanoantenna," *Physical Review Letters,* vol. 97, Jul 7 2006.

[90] L. Novotny and B. Hecht. (2012). *Principles of nano-optics (2nd ed.).*

[91] J. N. Farahani, D. W. Pohl, H. J. Eisler, and B. Hecht, "Single quantum dot coupled to a scanning optical antenna: A tunable superemitter," *Physical Review Letters,* vol. 95, Jul 1 2005.

[92] W. Kaiser and C. G. B. Garrett, "2-Photon Excitation in Caf2 : Eu2+," *Physical Review Letters,* vol. 7, pp. 229-231, 1961.

[93] D. R. Larson, W. R. Zipfel, R. M. Williams, S. W. Clark, M. P. Bruchez, F. W. Wise*, et al.*, "Water-soluble quantum dots for multiphoton fluorescence imaging in vivo," *Science,* vol. 300, pp. 1434-1436, May 30 2003.

[94] P. Bharadwaj and L. Novotny, "Robustness of Quantum Dot Power-Law Blinking," *Nano Letters,* vol. 11, pp. 2137-2141, May 2011.

[95] G. T. Boyd, Z. H. Yu, and Y. R. Shen, "Photoinduced luminescence from the noble metals and its enhancement on roughened surfaces," *Physical Review B,* vol. 33, pp. 7923-7936, 1986.

[96] V. P. Drachev, E. N. Khaliullin, W. Kim, F. Alzoubi, S. G. Rautian, V. P. Safonov*, et al.*, "Quantum size effect in two-photon excited luminescence from silver nanoparticles," *Physical Review B,* vol. 69, p. 035318, 2004.

[97] E. Castiglioni, S. Abbate, F. Lebon, and G. Longhi, "Chiroptical spectroscopic techniques based on fluorescence," *Methods and Applications in Fluorescence,* vol. 2, Jun 2014.

[98] N. I. Zheludev, A. D. Petrenko, Y. P. Svirko, and G. S. Filippova, "Nonlinear Optical-Activity in Weakly and Strongly Nonlinear Media - Direct and Cascade Processes - Bistability and Stochasticity," *Izvestiya Akademii Nauk Sssr Seriya Fizicheskaya,* vol. 48, pp. 603-610, 1984.

[99] O. V. Garibyan, B. V. Zhdanov, N. I. Zheludev, A. I. Kovrigin, and V. I. Kuznetsov, "Thermal Non-Linear Optical-Rotation in Cholesterol Liquid-Crystals," *Kristallografiya,* vol. 26, pp. 787-791, 1981.

[100] P. P. Markowicz, M. Samoc, J. Cerne, P. N. Prasad, A. Pucci, and G. Ruggeri, "Modified Z-scan techniques for investigations of nonlinear chiroptical effects," *Optics Express,* vol. 12, pp. 5209-5214, Oct 18 2004.

[101] S. I. L. Wawilow, W. L. , "Die Beziehungen zwischen Fluoreszenz und Phosphoreszenz in festen und flüssigen Medien," *Z. Physics.,* vol. 35, p. 16, 1926.

[102] S. A. Akhmanov and V. I. Zharikov, "Nonlinear Optics of Gyrotropic Media," *Jetp Letters-Ussr,* vol. 6, pp. 137-&, 1967.

[103] I. S. Zheludev, "Axial Tensors of 3rd Rank and Physical Effects They Describe," *Soviet Physics Crystallography, Ussr,* vol. 9, pp. 418-&, 1965.

[104] A. D. Petrenko and N. I. Zheludev, "Physical-Mechanisms of Nonlinear Optical-Activity in Crystals," *Optica Acta,* vol. 31, pp. 1177-1184, 1984.

[105] M. X. Ren, E. Plum, J. J. Xu, and N. I. Zheludev, "Giant nonlinear optical activity in a plasmonic metamaterial," *Nature Communications,* vol. 3, May 2012.